Mechanical Systems and Signal Processing 195 (2023) 110318

Contents lists available at ScienceDirect

Mechanical Systems and Signal Processing

journal homepage: www.elsevier.com/locate/ymssp

Real-time structural model updating using local eigenvalue modification procedure for applications in high-rate dynamic events

Emmanuel A. Ogunniyi [a,1], Claire Drnek [a,1], Seong Hyeon Hong [b], Austin R.J. Downey [a,c,*], Yi Wang [a], Jason D. Bakos [d], Peter Avitabile [e], Jacob Dodson [f]

[a] Department of Mechanical Engineering, University of South Carolina, United States of America
[b] Department of Mechanical and Civil Engineering, Florida Institute of Technology, United States of America
[c] Department of Civil and Environmental Engineering, University of South Carolina, United States of America
[d] Department of Computer Science and Engineering, University of South Carolina, United States of America
[e] Structural Dynamics and Acoustic Systems Laboratory, University of Massachusetts Lowell, United States of America
[f] Air Force Research Laboratory, United States of America

ARTICLE INFO

Communicated by S. Laflamme

MSC:
00-01
99-00

Keywords:
Real-time model updating
High-rate dynamics
Model reduction
Eigenvalue modification
Modal analysis
Adaptive structures

ABSTRACT

Estimating the state of structures that experience high-rate dynamics requires real-time model updating capabilities. High-rate dynamic events are characterized by (1) large uncertainties in the external loads, (2) high levels of non-stationarities and heavy disturbances, and (3) unmodeled dynamics generated from changes in system configurations. In order to achieve real-time model updating for high-rate dynamics, an algorithm should be able to update the structure's state on a timescale of 1 ms or less while circumventing pre-calculations to enable its operation over un-modeled event. This work formulates an algorithm to meet the stringent latency requirements using the local eigenvalue modification procedure (LEMP). In doing so, the model is transformed from the physical domain into the modal space which numerically simplifies the calculations needed to determine the state of a complex structure. To track the system through time, the structure's state is continuously updated by adjusting the associated model through online modal analysis. Its future states are estimated using a Bayesian search algorithm to compare the measured signals with selected modal models. New modal models are built based on the enhanced estimate of the structure's state and used for subsequent state estimations. The methodology is applied to an experimental testbed experiencing varying dynamics to update a surrogate model. Results show that the LEMP algorithm could update the state of the high-rate dynamics system within 1 ms for up to 250 nodes, a speed up of 125 times when compared to solving for the systems state using the generalized eigenvalue approach. The timing, accuracy, and computational resources are discussed in this paper and compared to the baseline generalized eigenvalue approach. An example problem and code are provided in a public repository.

1. Introduction

High-rate dynamics are defined as the dynamic responses of a system that are high-rate (<100 ms) and high-amplitude (acceleration > 100 g_n), such as those caused by a blast or impact [1]. Such events are complicated by instantaneous and

* Corresponding author at: Department of Mechanical Engineering, University of South Carolina, United States of America.
E-mail address: austindowney@sc.edu (A.R.J. Downey).
[1] Authors contributed equally.

https://doi.org/10.1016/j.ymssp.2023.110318
Received 11 October 2022; Accepted 21 March 2023
Available online 28 March 2023

unpredictable changes in the loading conditions acting upon a system, which alters the magnitude and location of internal and external forces experienced by the structure throughout the event. Because the changes experienced by the structure are sudden and unknown, tracking the state of the structure throughout the event remains a challenge.

One approach to tracking the state of such structures through a high-rate dynamic event is to utilize structural model updating techniques to update a digitized representation of the system state with real-time constraints. For accurate state estimations of structures experiencing high-rate dynamics, the model updating technique must: (1) be flexible to adapt to changing external load conditions without relying on pre-trained data and; (2) be capable of updating structural models within a 1 ms real-time latency constraints to enable real-time decision-making [2]. Model updating of structures using frequency-based methods is achieved using error minimization techniques [3,4]. In addition, frequency-based methods do not require exact knowledge of the input [5]. However, better performance and stability can be achieved when the input characteristics are either known or estimated [6].

Real-time model-updating enables tracking complex structures experiencing high-rate dynamic events such as in-flight monitoring systems and impact mitigation systems. In-flight monitoring can be applied to manned and unmanned aerial vehicles and spacecraft. In the case of an unmanned vehicle, where a pilot is not present to monitor the aircraft, operators on the ground must rely on sensor readings to determine the system's condition. Real-time model updating would allow the operating software to receive state data almost instantaneously, enhancing the knowledge of the system and its surroundings allowing for mission-critical actions [7]. In the case of manned vehicles, real-time model updating would allow for the incorporation of decision-making software that will respond to changing environments faster than human occupants can in a time of stress such as system or component failure [7].

Impact mitigation technology can be found in the defense and automotive industry, with examples including active blast mitigation systems and airbag deployment systems. Active blast mitigation systems minimize the blast's impact or counter the blast's effects after impact. Large forces associated with an incoming blast and close-range threats require the system to detect the presence of a blast threat, determine the magnitude and location of an incoming threat, and deploy countermeasures on a millisecond timescale [8]. Airbags are an essential safety component in vehicles; however, in some cases, the deployment of airbags can cause additional injuries to passengers. The Delphi Dual Depth airbag is an adaptive airbag that controls the extent of inflation based on factors such as the size and seated position of the passenger as well as the crash severity and location [9]. Real-time model updating would allow for additional adaptive measures, such as modifying the shape of an inflated airbag or adjusting the inflation rate to maximize protection within the latency constraints (i.e., allotted response time). In each application, real-time model updating would prioritize occupant's safety and mitigate the damage experienced by the system by providing users with the system's current state, thereby preventing further losses or failure.

Real-time model updating methodologies for structures have been developed for civil and aerospace structures by leveraging the Finite Element Analysis (FEA) [10–16]. However, the execution time requirements in these efforts were on the order of hours to months and often executed offline due to the computational costs associated with solving FEA models. Additionally, unmodeled dynamics characteristic of high-rate dynamic events limit the application of an FEA approach with pre-calculated databases of structural conditions for this class of structures [1]. The challenge of accounting for unmodeled dynamics necessitates the formulation of online model updating techniques that can track the system's state while requiring only a limited amount of offline training (e.g., the initial state of the structure). In prior work, the authors have experimentally demonstrated that real-time model updating can be accomplished for a structure undergoing a simulated high-rate event with a latency constraint of 1 ms using a simplified Euler–Bernoulli beam model and updating the model in the frequency domain [5]. However, to obtain the 1 ms latency constraint, the FEA model was limited to 23 nodes. In this configuration, 0.6 ms were required to solve the generalized eigenvalue problem, accounting for most of the computational load. Furthermore, the generalized eigenvalue formulation scales poorly for larger FEA models due to its $\mathcal{O}(n^3)$ complexity.

Real-time modeling in this work is accomplished using the local eigenvalue modification procedure (LEMP), which simplifies state calculations when only one change is made to the system [17] and a Bayesian probabilistic approach that reduces the search space. Advantages to applying LEMP are that all variables for the altered state are defined in terms of the initial state and changes made between the two. They only require information for the degrees of freedom (DOF) at which changes occur, which reduces the number of calculations required since the solution for the initial state equations is constant. Additionally, the original eigenvalue solution is reduced to a set of second-order equations through LEMP. Additional search space reduction is achieved by applying a Bayesian probabilistic approach that considers the current state of the structure given an initial uncertainty about the estimate itself [18]. A similar approach proposed by Madarshahian et al. [19] utilized a two-layer Bayesian approach to minimize the computational cost of estimating prior and posterior distributions. Huang et al. used the Bayesian learning to reconstruct signal from a compressive sensor to reduce the cost of signal transfer and storage [20], while Bayesian theory is used to produce the posterior joint probability distribution of the structure's physical properties in [21]. Moreover, Kurata et al. implemented a Bayesian approach conjointly with branch and bound search techniques to model the crack growth within aluminum hull structures [22].

The key contributions of this work are (1) the formulation of a real-time model updating technique that leverages an eigenvalue modification procedure to reduce the original eigenvalue problem to a set of second-order equations, and (2) the introduction of a Bayesian probabilistic approach for the sampling of potential structural states. Together, these advantages reduce the number and complexity of equations needed to compute the state of the structure and advance state-of-the-art structural model updating techniques for real-time applications with a latency constraint in the sub 1 ms range.

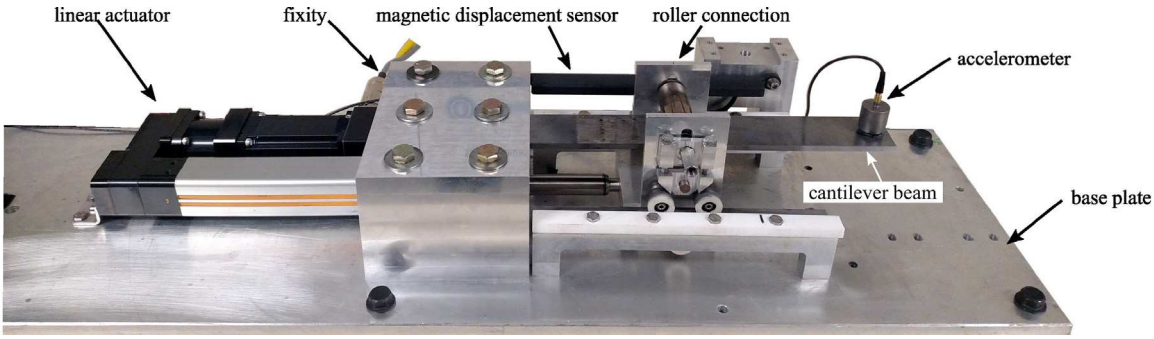

Fig. 1. DROPBEAR testbed as configured for this work.

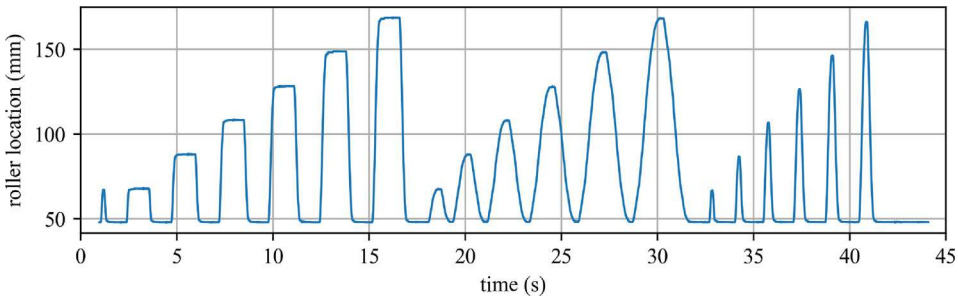

Fig. 2. Roller testing parameters used in this work.

2. Background

2.1. DROPBEAR experimental testbed

This work uses the DROPBEAR testbed, which was initially developed by Joyce et al. [23]. The DROPBEAR was constructed specifically for simulating high-rate dynamic events in the laboratory. It features two programmable changes: a detachable mass secured using an electromagnet and a movable roller boundary condition attached to a linear actuator, both used to simulate damage to the structure. The DROPBEAR testbed is advantageous when modeling high-rate dynamic cases because the setup is capable of repeatedly altering test parameters. These parameters can be changed during a test instead of between test runs, allowing researchers to gain insight into the system's real-time response. In this work, only the movable roller is utilized, and the algorithm is focused on its capability to model the nonstationary boundary conditions of the system. The experimental configuration used here is shown in Fig. 1.

The experimental configuration features an accelerometer (PCB Piezotronics model 393B04) mounted at the free end of a $51 \times 6 \times 350$ mm steel cantilever beam with a density of 7800 kg/m^3, Young's Modulus of 2e11 N/m^2 and Poisson's Ratio of 0.26. The design also features a sliding roller cart on a linear actuator that constrains vertical beam displacement between 48–17 mm from the fixed end and a magnetic displacement sensor that measures the roller's displacement throughout the test. Adjusting the roller location during tests simulates damage to the system by producing a user-defined change to the system input, which results in a change to a measured system output (e.g., acceleration). The use of rollers ensures the repeatability of each test, as the damage is simulated. This study investigates the reference data set initially presented in Downey et al. [5]. In this preliminary work, all results are obtained using the previously recorded sensor data. The measured test profile of the roller locations used in this work is presented in Fig. 2 and is open sourced; provided via a public repository [24].

2.2. Model development for the DROPBEAR experimental testbed

Initial state calculations are made using a finite element model and the Euler–Bernoulli beam theory. As shown in Fig. 3, the modified DROPBEAR testbed is modeled as a cantilever beam with the far-left end fixed and no additional support (i.e., no roller present). Each element has two nodes and 4 degrees of freedom (two rotation θ and two displacements υ). The beam is split into N elements of equal length resulting in $N + 1$ evenly spaced nodes along the beam. Two forces and two moments characterize an Euler–Bernoulli element, also shown in Fig. 3, resulting in $2(N + 1)$ DOF for the system.

The mass ($\mathbf{M}_i$) and stiffness ($\mathbf{K}_i$) matrices for an Euler–Bernoulli beam element can be found using Eqs. (1) and (2) as well as Table 1 which lists the material and geometric properties of the DROPBEAR testbed. These elemental matrices are combined to

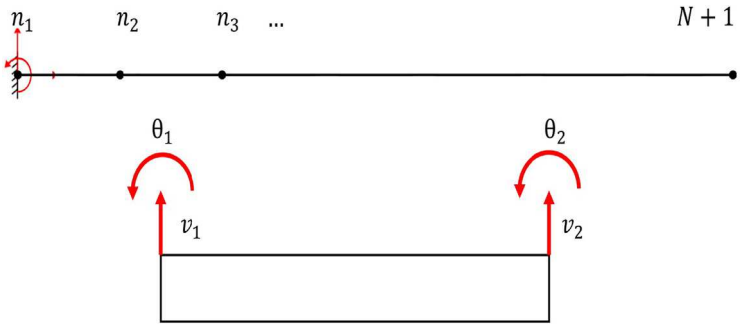

Fig. 3. DROPBEAR modeled as a cantilever Euler–Bernoulli beam.

Table 1
Material and geometric properties of the DROPBEAR testbed.

Density - ρ (kg/m^3)	7800
Cross-sectional area - A_c (m^2)	0.000306
Total length - l (m)	0.35
Elemental length - l_i (m)	0.35/N
Young's modulus - E (Pa)	2e11

construct the global mass ($\mathbf{M}_1$) and stiffness ($\mathbf{K}_1$) matrices for the initial sate.

$$\mathbf{M}_i = \frac{\rho_i A_i l_i}{420}\begin{bmatrix} 156 & 22l_i & 54 & -13l_i \\ 22l_i & 4l_i^2 & 13l_i & -3l_i^2 \\ 54 & 13l_i & 156 & -22l_i \\ -13l_i & -3l_i^2 & -22l_i & 4l_i^2 \end{bmatrix} \tag{1}$$

$$\mathbf{K}_i = \frac{E_i I_i}{l_i}\begin{bmatrix} 12/l_i^2 & 6/l_i & -12/l_i^2 & 6/l_i \\ 6/l_i & 4 & -6/l_i & 2 \\ -12/l_i^2 & -6/l_i & 12/l_i^2 & -6/l_i \\ 6/l_i & 2 & -6/l_i & 4 \end{bmatrix} \tag{2}$$

The equation of motion (EOM) for the entire system modeled as an Euler–Bernoulli beam is shown in Eq. (3) where $\mathbf{M}_1\ddot{x}$ and $\mathbf{K}_1 x$ are the mass and stiffness terms, respectively, for the initial system. The damping term ($\mathbf{C}\dot{x}$) can be ignored as its effect on the frequency of vibration is insignificant. The critical damping ratio (ζ) for the case when the roller is 48 mm distant from the support was found to be 0.0076 in experimental testing in Downey et al. [5]. As a result, the theoretical resonant frequency of the beam may be calculated using an impact excitation that excites all of the beam's frequencies equally. The predicted resonant frequency differs from the undamped natural frequency by only 0.005%. As a result, a simplified expression of the equation of motion that does not include the damping term can be utilized as follows:

$$\mathbf{M}_1\ddot{x} + \mathbf{K}_1 x = 0 \tag{3}$$

Here, $\ddot{x}$ and x are the acceleration and displacement vectors in physical space of length n. Additionally, $\mathbf{M}_1$ and $\mathbf{K}_1$ are the mass and stiffness matrices that are square symmetric and have dimensions of $n \times n$, where n is the DOF for the system.

By definition, the generalized eigenvalue (GE) problem for Eq. (3) is $\mathbf{K}_1\mathbf{U}_1 = \mathbf{M}_1\mathbf{U}_1\lambda$, where λ is a matrix of eigenvalues and $\mathbf{U}_1$ is the matrix of eigenvectors, both having dimensions of $n \times n$. The GE problem can be solved using Eqs. (4) and (5) below.

$$\det[\mathbf{K}_1 - \lambda\mathbf{M}_1] = 0 \tag{4}$$

$$[\mathbf{K}_1 - \lambda\mathbf{M}_1]\mathbf{U}_1 = 0 \tag{5}$$

Solutions to the previous equations yield eigenvalues and eigenvectors according to Eqs. (6) and (7) respectively. Eigenvalues are related to the natural frequency of the system, while eigenvectors are related to mode shapes of the system and are assembled in matrix form as:

$$\lambda = \begin{bmatrix} \omega_1^2 & 0 & 0 & 0 \\ 0 & \omega_2^2 & 0 & 0 \\ 0 & 0 & \ddots & 0 \\ 0 & 0 & 0 & \omega_n^2 \end{bmatrix} \tag{6}$$

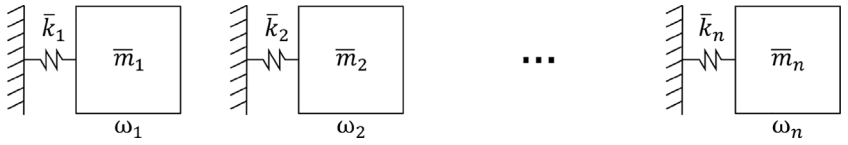

Fig. 4. Modal representation of initial system.

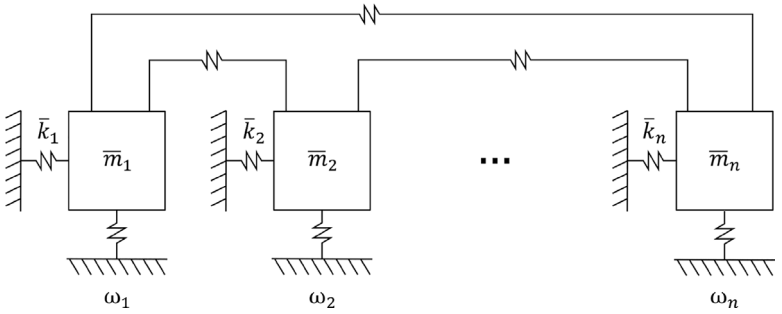

Fig. 5. Modal representation of altered system.

$$\mathbf{U}_1 = \left[\vec{u}_1^1 \quad \vec{u}_2^1 \quad \dots \quad \vec{u}_n^1\right] \tag{7}$$

where ω_n and $\vec{u}_n^1$ are the nth frequency and modal vector for the initial state of the system where the arrow denotes a vector. Although the modal matrix does not represent system mode shapes, it can be used to calculate them.

2.3. Local eigenvalue modification procedure

Structural dynamic modification (SDM) identifies physical modifications made to system properties such as mass, stiffness, or damping by monitoring changes in the system's dynamic response such as frequencies and mode shapes or vice versa [25–28]. SDM is accomplished by modeling the altered state as a combination of the initial state and the changes between the states using changes to mass, stiffness, or damping matrices in the EOM for the altered system. SDM also utilizes the principle of modal synthesis, which states that any dynamic response of a vibrating structure can be decomposed into a set of individual contributions of single frequencies [29,30]. Also, it effectively defines the initial system of n DOF as a set of n independent single DOF systems, as illustrated in Fig. 4. This is done by utilizing the relationship between the modal properties and spatial properties of a structure, which simplifies state estimations for complex systems by transforming equations from physical space to modal space using the GE solution of the initial state [25,26].

In Fig. 4, each DOF responds to one natural frequency of the physical system with a modal mass and stiffness value related to physical system response through modal transformations. Any changes made to this initial system result in an altered modal system. These changes (e.g., mass and stiffness) can be transformed into modal space where matrix values on the diagonal represent a mass or stiffness change from the initial system (i.e., Fig. 4) to ground, and off-diagonal values in the matrix couple individual systems together as shown in Fig. 5 by the connecting springs.

One advantage of operating in modal space is that the model for the initial structure only needs to contain information for the DOF where modifications are made, thereby reducing the size of the matrices in the EOM, and the number of corresponding calculations required [31,32]. Therefore, solving the reduced EOM in modal space requires processing a smaller GE solution to find the model's new frequencies and mode shapes. While this reduces the computational cost compared to solving the original GE, it still requires solving a GE problem which may still be too computationally expensive given the stringent timing constraints demanded by the high-rate dynamics problem [33].

Weissenburger originally developed LEMP in 1968 to avoid eigenvalue solutions in SDM when the system undergoes a single change. The idea was to simplify state calculations to meet the limited processing power of computers at the time [17,34–36]. Following the initial modification, the system equations had to be updated, and other additional modifications had to be performed; this was a time-consuming procedure. LEMP utilizes a single GE solution for the initial system and simplifies altered state equations by transforming them into modal space, isolating the DOFs that contribute to the changes between states, and defining equations in terms of the initial state as discussed in SDM. However, additional simplifications occur by truncating the n independent single degree of systems to only include the m modes of interest. This results in a λ matrix with dimensions $m \times m$ and a corresponding modal matrix $\mathbf{U}_1$ of dimensions $n \times m$. This modal truncation further simplifies the altered state equations. An overview of the LEMP is shown in Fig. 6 and will be discussed further in the following sections.

The benefit of applying LEMP is that the GE equation is reduced to a set of second-order equations whose frequency roots are bounded by the initial frequencies of the system, thereby reducing the domain over which the equation is solved [17]. These

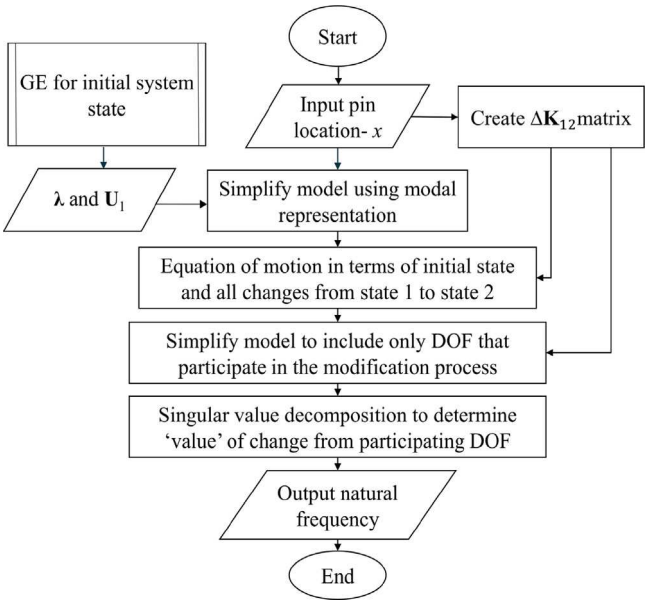

Fig. 6. Flowchart of LEMP algorithm.

simplifications reduce the number and complexity of equations needed to compute the structure's state, equating to less computing time than the previously mentioned GE solutions.

Accelerating computations would allow for more complex models such as those with additional nodes or various element types. More complex models would significantly enhance the usefulness of physics-informed state estimation of structures experiencing high-rate dynamic events. Moreover, these high-quality models are critical to performing prognostics and enabling decision-making for these structures.

2.4. Search space reduction

The search space for comparison points between the actual and estimated state is reduced by defining an adaptive standard deviation (SD) equal to the percentage error found in the frequency domain, as shown in Eq. (8). This technique for altering the size of a search space is adopted from Hong et al. [37]. Altering the size of a search space is advantageous because it allows for expanding search locations when the sampled states differ from the measured states, enabling the algorithm to estimate sudden changes in the system. It also reduces search locations when sampled and measured states are similar, enabling the algorithm to model a constant system without much variation.

$$\sigma = \frac{\omega_{\text{estimate}}^{\text{previous}} - \omega_{\text{true}}^{\text{current}}}{\omega_{\text{true}}^{\text{current}}} \tag{8}$$

Here, σ is the SD of a normal distribution about the last roller position, $\omega_{\text{true}}^{\text{current}}$ is the current measured frequency from experimental data and $\omega_{\text{estimate}}^{\text{previous}}$ is the previously estimated frequency. Eq. (8) assumes that the percentage error in frequency is equivalent to the percentage error in position; however, since roller location and frequency are not linearly related, this assumption is not necessarily true for every case. It should be a good approximation when the estimate approaches the true value.

Additional search space reduction is achieved by applying a Bayesian probabilistic approach. Bayesian approaches are frequently utilized in structural health monitoring applications due to their simplicity, adaptability, and updatable nature [38–41]. Bayesian approaches are implemented to assess the estimate of the state of the structure given an initial uncertainty about the estimate itself [18,42]. The Bayesian approach is capable of accounting for uncertainty in the individual predictions (or estimates) made by a model, and the uncertainty in the model fits itself [18]. Bayesian approaches are advantageous because they can be combined with other data analysis techniques to improve statistical results further and can be easily implemented into experimental analysis without changing lab setups.

In this work, each state estimate contains a level of uncertainty that is accounted for here by utilizing the likelihood function, which represents the error between the actual measured structure and the LEMP estimated model [43]. In other words, when a new roller location is estimated, that value becomes the mean around which a new Gaussian distribution is created. Values from the updated probability density function (PDF) are selected and either accepted or rejected using the likelihood function and Bayes equation. These points are then used as comparison points for future state estimations. By limiting the search space for comparison points, the adaptive standard deviation and Bayesian approach allow for better selection, thereby reducing the number of comparison points needed.

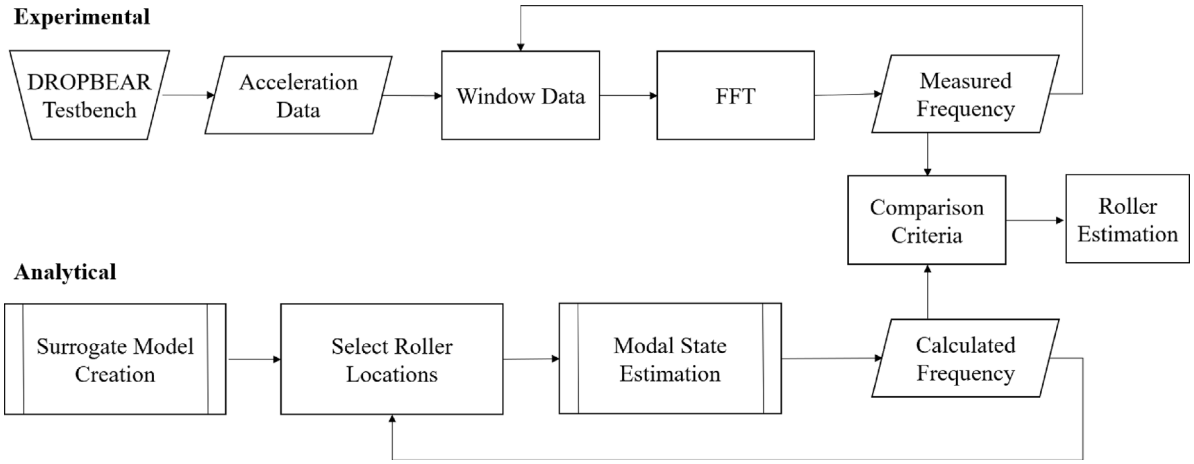

Fig. 7. Flowchart of overall procedure used in this work.

3. Methodology

The proposed real-time model updating algorithm is divided into three main parts: experimental, analytical, and model creation. The analytical procedure is further separated into two procedures: computing the modal state estimation using LEMP and selecting roller locations using the Bayesian search space. The overall procedure is shown in Fig. 7.

3.1. Experimental

The experimental procedure aims to determine the true system response of the DROPBEAR testbed with varying boundary conditions. This is accomplished by collecting acceleration data from the system using the accelerometer mounted on the beam's free end. Before the acceleration data is processed, a sliding Hann window is applied to smooth the time-series data. The beam's natural frequency is then obtained by taking the Fast Fourier Transform (FFT) of the acceleration data. This measured system response is then compared to the various analytically solved models, and state estimation is made using comparison methods for the frequency of the first mode of the structure.

3.1.1. LEMP algorithm

LEMP is applied according to the process illustrated in Fig. 6. After the GE solution is obtained for the initial system, the EOM for the altered state is created according to Eq. (9) while ignoring the effects of damping.

$$\mathbf{M}_2\ddot{x} + \mathbf{K}_2 x = 0 \tag{9}$$

where $\mathbf{M}_2$ and $\mathbf{K}_2$ are the mass and stiffness matrices of the altered state in physical space, both with dimensions of $n \times n$. In this work, the change between system states results from adding a roller boundary condition at a node location along the beam. In traditional FEA approaches, the application of a roller limiting bending in the beam at that location allows for row and column cancellation. Instead, here we assume a large numerical stiffness (K = 10,000 N/m) for the roller at a given node position, allowing for calculations using a full matrix without varying the resulting state calculations. Therefore, there is no change made to the mass matrix, only a change made to the stiffness matrix, denoted by $\Delta\mathbf{K}_{12}$ with dimensions of $n \times n$. The mass and stiffness of the altered state are defined in terms of the initial state and changes between the two as shown in Eqs. (10) and (11) respectively.

$$\mathbf{M}_2 = \mathbf{M}_1 \tag{10}$$

$$\mathbf{K}_2 = \mathbf{K}_1 + \Delta\mathbf{K}_{12} \tag{11}$$

Substituting Eqs. (10) and (11) into the original EOM for the altered state yields Eq. (12).

$$\mathbf{M}_1\ddot{x} + (\mathbf{K}_1 + \Delta\mathbf{K}_{12})x = 0 \tag{12}$$

To simplify future calculations, the n modes of the n independent single DOF systems of the initial system are truncated to only include the m modes of interest. This results in λ matrix with dimensions $m \times m$ and a corresponding modal matrix $\mathbf{U}_1$ of dimensions $n \times m$. This modal truncation further simplifies the altered state equations. Additional simplifications occur by transforming the system response from physical space to modal space using the relations shown in Eqs. (13) and (14), where p_1 and $\ddot{p}_1$ are the system displacement and acceleration vectors in modal space whose length is reduced from n to m after modal truncation occurs.

$$x = \mathbf{U}_1 p_1 \tag{13}$$

$$\ddot{x} = \mathbf{U}_1 \ddot{p}_1 \tag{14}$$

Converting the EOM to modal space utilizing Eqs. (13) and (14) yields Eq. (15) below.

$$\mathbf{M}_1\mathbf{U}_1\ddot{p}_1 + (\mathbf{K}_1 + \Delta\mathbf{K}_{12})\mathbf{U}_1 p_1 = 0 \tag{15}$$

By multiplying each term by $\mathbf{U}_1^{\mathrm{T}}$ the mass and stiffness matrices are normalized in modal space which yields diagonal matrices as shown in Eq. (16).

$$\mathrm{diag}(\overline{\mathbf{M}}_1)\ddot{p}_1 + [\mathrm{diag}(\overline{\mathbf{K}}_1) + \Delta\overline{\mathbf{K}}_{12}]p_1 = 0 \tag{16}$$

where $\overline{\mathbf{M}}_1$ and $\overline{\mathbf{K}}_1$ represent the modal mass and stiffness matrices and $\Delta\overline{\mathbf{K}}_{12}$ represents the changes made in modal space between the initial and altered state. These matrix dimensions are reduced from $n \times n$ to $m \times m$ after modal truncation occurs. Diagonal values of $\Delta\overline{\mathbf{K}}_{12}$ represent ground connections and off-diagonal values couple the single DOF systems as shown between Figs. 4 and 5. Note the overline on $\Delta\overline{\mathbf{K}}_{12}$ in Eq. (16) which is the change made in modal space is different from $\Delta\mathbf{K}_{12}$ in Eq. (15) which is the change made in physical space.

Scaling Eq. (16) to unit modal mass yields Eq. (17), where $\mathbf{I}$ is the identity matrix with dimensions of $m \times m$. The benefit of scaling to modal mass is that the state equation for the altered state in modal space can be written in terms of the initial eigenvalues, which were already obtained by Eq. (6). Also note that the $\Delta\overline{\mathbf{K}}_{12}$ in Eq. (17) is different from that in Eq. (16) as it has been scaled to unit modal mass.

$$\mathbf{I}\ddot{p}_1 + [\lambda + \Delta\overline{\mathbf{K}}_{12}]p_1 = 0 \tag{17}$$

To solve for the updated natural frequencies that occur as a result of system changes, the following procedure is implemented. First, the GE solution of Eq. (17) is set up, but not solved according to Eqs. (18) and (19) below.

$$\det[(\lambda + \Delta\overline{\mathbf{K}}_{12}) - \boldsymbol{\Lambda}\mathbf{I}] = 0 \tag{18}$$

$$[(\lambda + \Delta\overline{\mathbf{K}}_{12}) - \boldsymbol{\Lambda}\mathbf{I}]p_{12} = 0 \tag{19}$$

$\boldsymbol{\Lambda}$ is a matrix with dimensions of $m \times m$ whose the diagonals are the squares of the updated frequencies and p_{12} is the modal change between the states. The terms are then rearranged to yield Eq. (20).

$$[(\lambda - \boldsymbol{\Lambda}) + \Delta\overline{\mathbf{K}}_{12}]p_{12} = 0 \tag{20}$$

Because the stiffness change between states occurs as a result of applying a nodal boundary condition, only diagonal values will be affected between the $\mathbf{K}_1$ and $\mathbf{K}_2$ matrices. Furthermore, the only non-zero term in the $\Delta\mathbf{K}_{12}$ matrix is the diagonal value associated with the DOF where the roller is located. Noting that the only non-zero values in $\Delta\mathbf{K}_{12}$ are those associated with the DOF(s) that experience a change in stiffness from the initial to an altered state. The equation for $\Delta\overline{\mathbf{K}}_{12}$ is then simplified to only contain information from the contributing nodes. This is accomplished through spectral decomposition of $\Delta\mathbf{K}_{12}$ as shown in Eq. (21).

$$\Delta\mathbf{K}_{12} = \mathbf{T}\mathrm{diag}(\boldsymbol{\alpha})\mathbf{T}^{\mathrm{T}} \tag{21}$$

where $\mathbf{T}$ is the $n \times n$ tie matrix consisting of a set of row tie vectors as shown in Eq. (22) and $\boldsymbol{\alpha}$ is a matrix of size n obtained from the single value decomposition of $\Delta\mathbf{K}_{12}$. The tie matrix represents connections between the two system's states while the alpha value is the singular change in the stiffness.

$$\mathbf{T} = \begin{bmatrix} \vec{t}_1 & \vec{t}_2 & \cdots & \vec{t}_n \end{bmatrix}^{\mathrm{T}} \tag{22}$$

Eq. (21) is then transformed to modal space by multiplying each side by $\mathbf{U}_1$ and $\mathbf{U}_1^{\mathrm{T}}$ as shown in Eq. (23).

$$\Delta\overline{\mathbf{K}}_{12} = \mathbf{U}_1^{\mathrm{T}}\mathbf{T}\mathrm{diag}(\boldsymbol{\alpha})\mathbf{T}^{\mathrm{T}}\mathbf{U}_1 \tag{23}$$

The contributing values of $\Delta\overline{\mathbf{K}}_{12}$ can be redefined by reducing $\Delta\mathbf{K}_{12}$ to only include non-zero values which is denoted by $\Delta\mathbf{k}_{12}$. This is done by using the tie vector and alpha value associated with the affected DOF, denoted by t_c and α respectively. $\Delta\mathbf{k}_{12}$ can then be transformed to modal space utilizing the corresponding rows of $\mathbf{U}_1$, denoted by $\mathbf{U}_{1_c}$. These reduced matrices only include information associated with the DOF(s) experiencing a stiffness change and are obtained using the relation in Eq. (24) where $\vec{v}$ is the one-dimensional contribution vector, of length m, associated with the affected DOF as noted in Eq. (25).

$$\vec{v} = \mathbf{U}_{1_c}^{\mathrm{T}}\vec{t}_c \tag{24}$$

$$\vec{v} = \begin{bmatrix} \mathrm{v}_1 & \mathrm{v}_2 & \cdots & \mathrm{v}_m \end{bmatrix}^{\mathrm{T}} \tag{25}$$

The relation from Eq. (24) is then used along with the alpha value associated with the affected DOF to solve for $\Delta\bar{\mathbf{k}}_{12}$. This is done according to Eq. (26) which yields the equation for the modal stiffness change in terms of contributing nodes only.

$$\Delta\bar{\mathbf{k}}_{12} = \vec{v}\,\alpha\,\vec{v}^{\mathrm{T}} \tag{26}$$

Noting that $\Delta\bar{\mathbf{k}}_{12}$ is equivalent to $\Delta\overline{\mathbf{K}}_{12}$, and of dimension $n \times n$, Eq. (26) can be substituted for $\Delta\overline{\mathbf{K}}_{12}$ in the original GE problems shown in Eqs. (18) and (19) which yields the following equations:

$$[(\lambda - \boldsymbol{\Lambda}) + \vec{v}\,\alpha\,\vec{v}^{\mathrm{T}}]p_{12} = 0 \tag{27}$$

$$(\lambda - \boldsymbol{\Lambda})p_{12} + \vec{v}\,\alpha\,\vec{v}^{\mathrm{T}}p_{12} = 0 \tag{28}$$

To further simplify state equations, $\mathbf{S}$ is defined as an arbitrary variable according to Eq. (29).

$$\mathbf{S} = \vec{v}^{\mathrm{T}}p_{12} \tag{29}$$

Eq. (29) is then substituted into Eq. (28) to yield Eq. (30).

$$(\lambda - \boldsymbol{\Lambda})p_{12} + \vec{v}\alpha\mathbf{S} = 0 \tag{30}$$

Which can be rearranged to solve for p_{12} as shown in Eq. (31)

$$p_{12} = -(\lambda - \boldsymbol{\Lambda})^{-1}\,\vec{v}\alpha\mathbf{S} \tag{31}$$

Then, Eq. (31) is multiplied by $\vec{v}^{\mathrm{T}}$ to yield Eq. (32)

$$\vec{v}^{\mathrm{T}}p_{12} = -\vec{v}^{\mathrm{T}}(\lambda - \boldsymbol{\Lambda})^{-1}\,\vec{v}\alpha\mathbf{S} \tag{32}$$

Which can be rewritten as Eq. (33) using the relation from Eq. (29)

$$\mathbf{S} = -\vec{v}^{\mathrm{T}}(\lambda - \boldsymbol{\Lambda})^{-1}\,\vec{v}\alpha\mathbf{S} \tag{33}$$

By multiplying each side by $\mathbf{S}^{-1}$, both $\mathbf{S}$ matrices are eliminated leaving the matrix equation shown in Eq. (34).

$$\alpha^{-1} = -\vec{v}^{\mathrm{T}}(\lambda - \boldsymbol{\Lambda})^{-1}\,\vec{v} \tag{34}$$

Since $\vec{v}$ is a one-dimensional vector, $\vec{v}$ is element-wise equal to $\vec{v}^{\mathrm{T}}$. Therefore, breaking Eq. (34) into components yields the following equation, where the only unknown is Ω_r or the natural frequency of the altered system. Here, r ranges from 1 to m, where m is the number of modes used to describe the system. The LEMP algorithm results in a secular equation of Eq. (35) solved using the divide and conquer approach described in [44].

$$\frac{-1}{\alpha} = \sum_{r=1}^{m} \frac{v_r^2}{\omega_r^2 - \Omega_r^2} \tag{35}$$

In summary, LEMP consists of two main parts: a single GE solution for the initial state of the system and an eigenvalue modification process for the altered system state that is updated for each roller position. The eigenvalue modification process consists of simplifications to state equations accomplished by defining the system in terms of the initial state and changes made between the two states, utilizing modal representation, and isolating contributing nodes.

3.1.2. Model creation

As previously noted, additional simplifications occur within LEMP by truncating the n independent single DOF systems to only include the m modes of interest. However, this process requires the creation of a pre-selected surrogate model, which includes determining the number of modes and nodes to use when modeling the system. The goal is to include enough information about the system to ensure the state estimate contains a minimal error without including excess information that negatively affects computation time.

Not all initial modes will contribute equally to altered frequencies, but missing modes that do contribute will drastically increase the estimation error due to truncation. Therefore, predetermining which initial modes contribute and how much each contributes to the altered states is essential. This is accomplished by solving for modal transformation matrix $\mathbf{U}_{12}$, of dimensions $n \times n$, which uncouples the modification between states. Recall from the altered EOM in modal space, as shown by Eq. (16), that p_1 and $\ddot{p}_1$ are initial system displacement and acceleration in modal space of initial length n. The initial modal response can also be rewritten as a function of the modal response of the altered state and the modal transformation matrix according to the following relations:

$$p_1 = \mathbf{U}_{12}p_2 \tag{36}$$

$$\ddot{p}_1 = \mathbf{U}_{12}\ddot{p}_2 \tag{37}$$

where p_2 and $\ddot{p}_2$ are also of length n. If LEMP were not applied, the GE solution of Eq. (16) given the transformation shown in Eqs. (36) and (37) could be solved using Eq. (38) below.

$$\{[\mathrm{diag}(\overline{\mathbf{K}}_1) + \Delta\overline{\mathbf{K}}_{12}] - \lambda_{12}\mathrm{diag}(\overline{\mathbf{M}}_1)\}\mathbf{U}_{12} = 0 \tag{38}$$

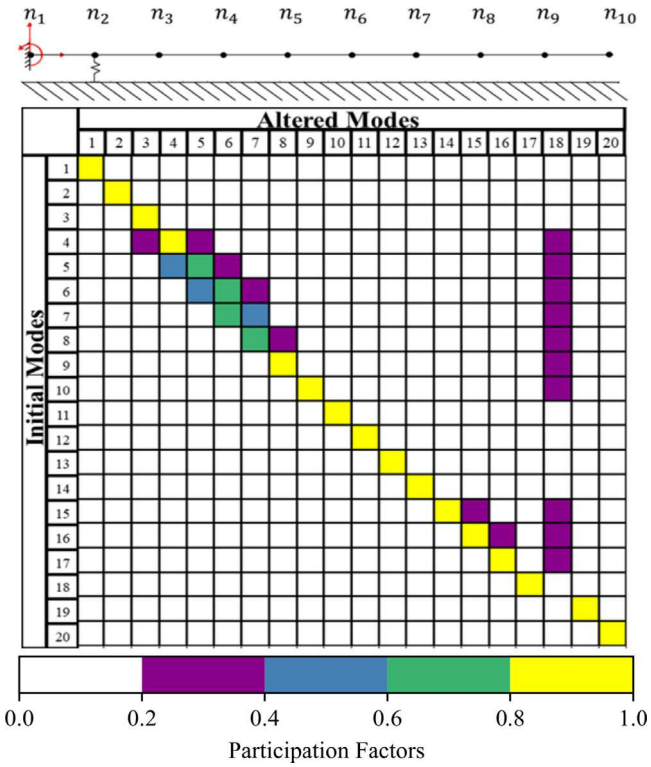

Fig. 8. Modal participation factors for the altered state with roller at n_2.

where Eq. (38) is generalized eigenvalue solution for equation Eq. (16) and λ_{12} is the eigenvalue. The eigenvectors of Eq. (38) are the columns of matrix $\mathbf{U}_{12}$ and are called participation factors. These values offer insight into each initial mode's weight in defining the altered modes. Values range between −1 and 1, where absolute values closer to 1 correspond with a larger modal contribution.

In the case of this work, the modal response of the initial system is that of a cantilever beam, and the addition of a roller alters modal responses. To determine the participation factors of the system used here, the number of nodes was initially set to 10, which corresponds to 20 DOFs due to the characterization of the system as an Euler–Bernoulli beam (yielding a 20×20 $\mathbf{U}_1$ matrix). The participation factors were calculated at each node along the beam, excluding the fixed end, and plotted according to the key in Fig. 8. The participation factors were not calculated for the node at the fixed end because the system is already constrained in the bending and rotational DOF due to the boundary condition; therefore, adding a roller would not change the system response.

Figs. 8–10 illustrate the modal participation factors for a roller located at nodes ranging along the beam. The initial modes of the cantilever beam are listed on the vertical axes, and altered modes of the cantilever beam with a roller placed at a node are listed along the horizontal axes. Boxes are color-coded based on the value of the participation factor, where white boxes represent little to no contribution and yellow represents high levels of contribution. For example, in Fig. 8, the altered modes (horizontal axis) are the modes for the system when the pin is at the second node. In this case, the fifth mode for the altered shape can be represented as a combination of modes 4, 5, and 6 from the initial cantilever beam with participation factors of 0.2383, 0.7717, and 0.5489, respectively. Future analysis will focus on contributions greater than 0.2 from initial modes.

Using Figs. 8–10, the contributions from initial modes were tallied based on participation factors. The total counts and contribution percentage for initial modes whose contribution factors were greater than 0.2 are summarized in Table 2.

Participating modes were selected if their contribution percentage was significant (5% or greater). Therefore, initial modes 1–9 and 12 were selected. Additional limitations due to the experimental setup and accelerometer selection further reduced the selected modes. In order to utilize a mode in state estimations, the data acquisition system must be capable of measuring that mode experimentally. Therefore, each mode type and frequency must be considered when selecting modes. Mode shapes and natural frequencies are shown for all participating modes in Fig. 11.

The experimental setup in this work utilizes a single-axis accelerometer mounted at the far end of the beam, which limits measurable modes to those of bending in the Y direction. Additionally, the maximum frequency range of the accelerometer was (±3 dB) 0.02–1700 Hz [45]. Therefore, the modes used to describe the system were limited to modes 1–4.

The number of nodes determines how refined the solution is, with more nodes offering a more accurate estimation but requiring a longer calculation time and fewer nodes saving time but offering rougher estimates. The first four natural frequency responses are plotted as the roller moves along the beam for models with varying node numbers to determine the number of nodes required. The true frequency is defined using LEMP with 101 nodes, then compared to reduced models containing 51, 26, and 21 nodes. The

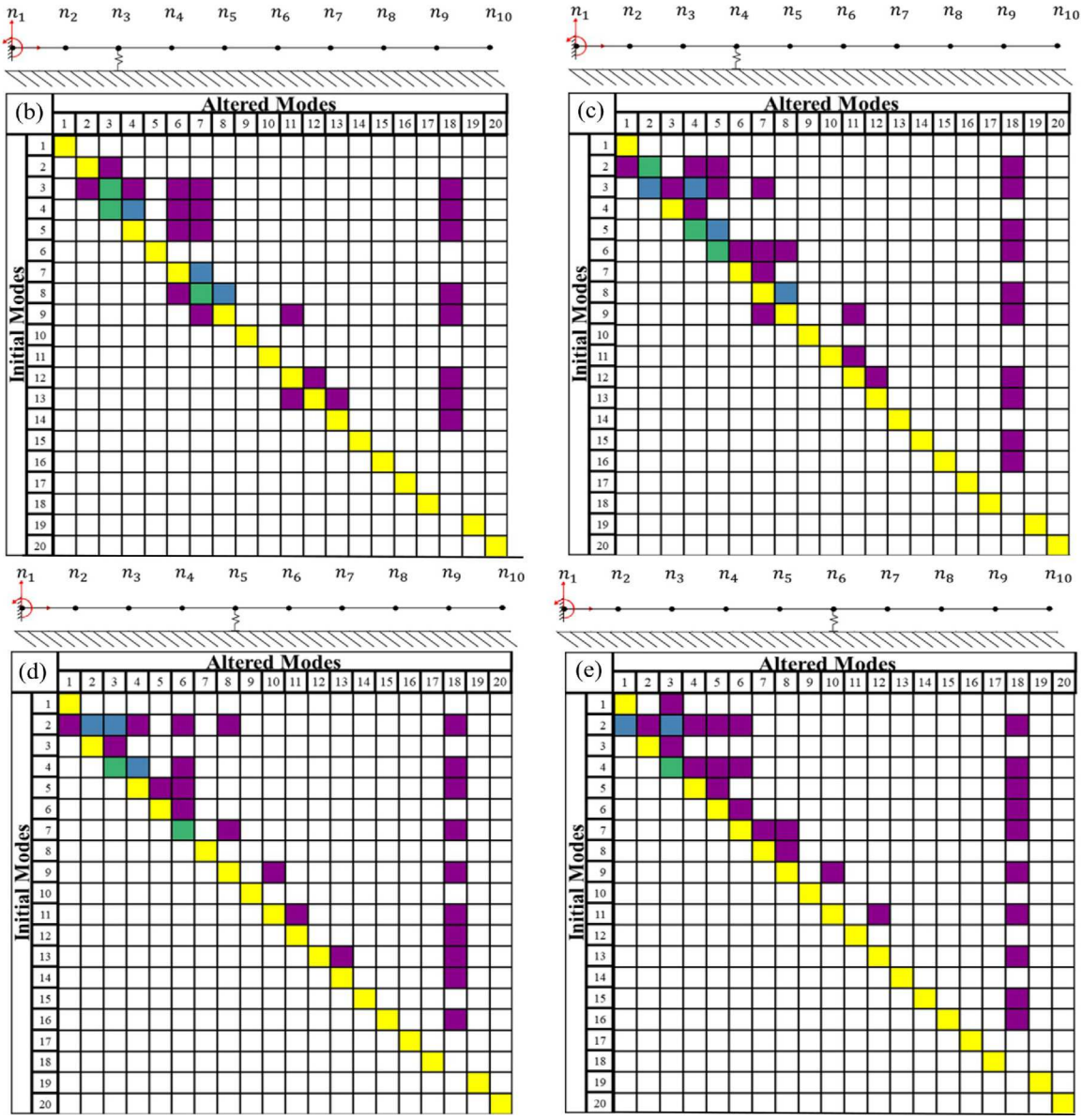

Fig. 9. Modal participation factors for the altered state with roller at n_3 (b), n_4 (c), n_5 (d), and n_6 (e).

relative error between the true and reduced models increases as the number of nodes decreases and exceeds the maximum allowable error of 10 mm when the number of nodes is reduced to 21. Therefore, the reduced model with 26 nodes is selected to represent the system. The first four natural frequencies of the system plotted using the selected 26-node reduced model are shown in Fig. 12. Fig. 12 represents a horizontal error (mm) between the two models estimated roller position, and as observed, the 26 nodes model lags the 101 nodes model, as opposed to a vertical error (Hz), on which the 26-node model consistently overestimates the frequency when the roller is located near the fixed end, jumps in error levels out as the roller moves along the beam. Furthermore, it was shown in Downey et al. in Ref. [5] that a 26 node FEA model could be solved in 2 ms using the GE approach, and Ogunniyi et al. also showed in Ref. [44] that a 26 node FEA model could be solved in less than 1 ms using the LEMP approach.

3.1.3. Roller location selection

In this work, the high-rate dynamic system is represented by the FEA model. Three roller locations are sampled using a normal probability density function according to Fig. 13, where the mean of the distribution is the center of the beam before the estimation process starts. After each successive iteration process, the mean of the distribution changes to the previous roller location. The mean, μ, and the standard deviation, σ, are used to sample the three roller locations. The two remaining roller locations are selected above

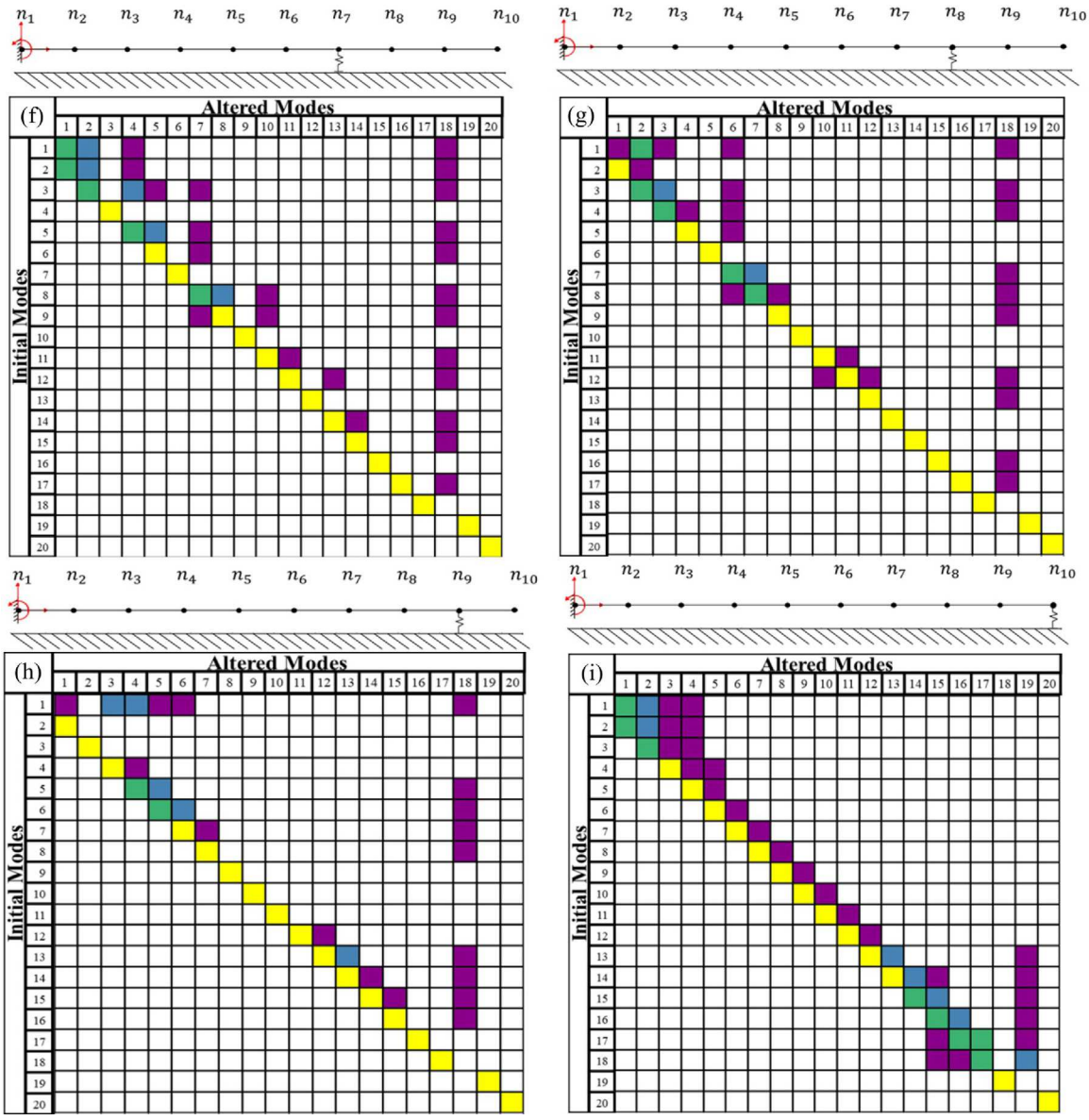

Fig. 10. Modal participation factors for the altered state with roller at n_7 (f), n_8 (g), n_9 (h) and n_{10} (i).

the mean since the roller is assumed to be always moving to the right. Three FEA models are built using these roller locations, then all three models' first natural frequencies are obtained by doing a modal analysis on them simultaneously $(\omega_1, \omega_2, \omega_3)$. In order to determine the location of the roller, the measured frequency (ω_{true}) of the real system, which was derived from the FFT of the accelerometer data, is compared with $(\omega_1, \omega_2, \omega_3)$. The PDF algorithm that was used to sample the sites is then modified considering comparisons between the estimated roller location and frequency. By contrasting the natural frequencies derived from the experiments and the FEA models and creating new FEA models based on the improved estimate of the position, it is possible to narrow down the determination of the roller position constantly.

Bayesian search space for roller location selection

The function of the Bayesian probabilistic approach is to select the most probable roller locations at which to apply LEMP. This selection improves initial estimations and reduces the number of comparison points selected and the required error calculations. Fig. 13 illustrates the Bayesian procedure applied in this work.

Let R denote the hypothesis that the roller is moving from left to right along the beam. It is initially assumed that the roller is located at the center of the beam and is moving right with a probability $P(R) = .6$ (therefore $P(L) = .4$); all future calculations

Mode	Frequency (Hz)	Mode type	Shape
1	37.6956	Bending-Y	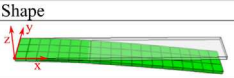
2	248.561	Bending-Y	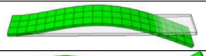
3	713.463	Bending-Y	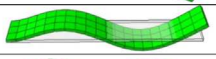
4	1416.40	Bending-Y	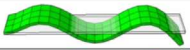
5	2353.62	Bending-Y	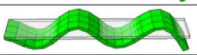
6	3519.66	Bending-Z	
7	4918.50	Torsional	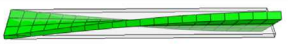
8	6569.90	Bending-Y	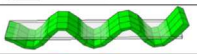
9	8422.02	Bending-Y	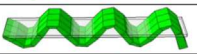
12	15420.6	Torsional	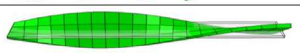

Fig. 11. Participating mode shapes and natural frequencies.

Table 2
Counts and percentages for contributing initial modes.

Contributing mode	Yellow (0.8–1)	Green (0.6–0.8)	Blue (0.4–0.6)	Purple (0.2–0.4)	Total counts	Contribution percentage (%)
1	5	2	6	13	26	6.3725
2	4	4	4	18	30	7.3529
3	4	3	6	20	33	8.0882
4	6	2	1	14	23	5.6372
5	2	7	7	15	31	7.5980
6	4	5	3	18	30	7.3529
7	8	1	2	10	21	5.1470
8	5	4	4	13	26	6.3725
9	9	0	1	18	28	6.8627
10	9	0	0	1	10	2.4509
11	9	0	0	8	17	4.1666
12	9	0	0	12	21	5.1470
13	9	0	2	8	19	4.6568
14	9	0	0	9	18	4.411
15	9	0	0	11	20	4.9019
16	9	0	0	7	16	3.9215
17	9	0	0	3	12	2.9411
18	9	0	0	0	9	2.2058
19	9	0	0	0	9	2.2058
20	9	0	0	0	9	2.2058

assess the probability that the roller will continue to move right. Weighting initial directional probabilities is equivalent to making predictions about how a system will degrade based on previous knowledge. For example, when modeling structures, the equivalent stiffness will decrease over time as the structure degrades; therefore, the initial weighted prediction and future estimations would assess a decrease in stiffness.

Three roller locations are sampled as comparison points given a PDF of normal distribution centered on the previous roller position. The first location is taken to be the previous mean (μ_B), assuming that there is no damage occurring between the two estimations. A random location (x) is chosen above the mean value. The likelihood functions for the selected point (x) are calculated according to the two previous distributions, Eqs. (39) and (40) respectively. Here B represents the previous distribution, and A represents the distribution prior to that. As the roller is assumed to always move to the right, the distribution prior to the previous is always to the left of the previous distribution; except when the posterior distribution $P(R \mid E) > 0.5$.

$$P(E \mid R) = \frac{1}{\sqrt{2\pi\sigma^2}} \exp \frac{-1}{2} \frac{(x-\mu_B)^2}{2\sigma^2} \tag{39}$$

$$P(E \mid L) = \frac{1}{\sqrt{2\pi\sigma^2}} \exp \frac{-1}{2} \frac{(x-\mu_A)^2}{2\sigma^2} \tag{40}$$

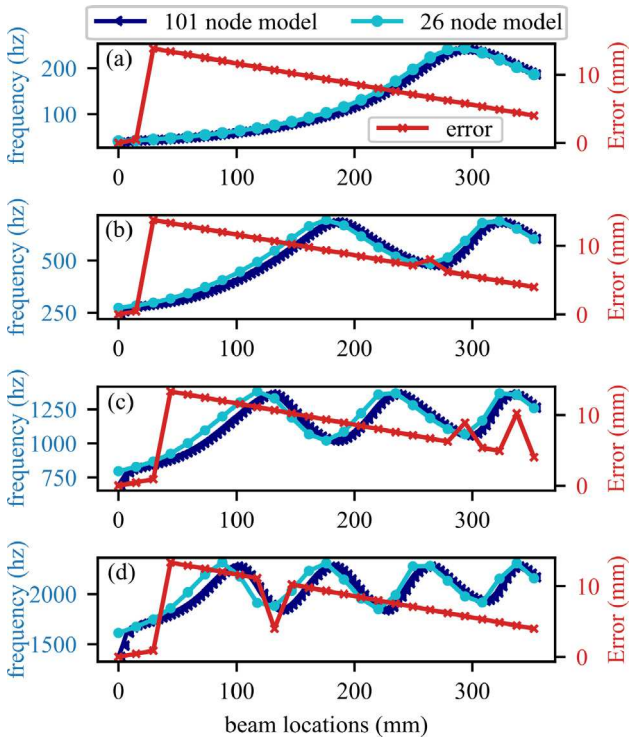

Fig. 12. First four frequency responses for a 26 node model solved using the LEMP process along with the reference 101 node model and the error.

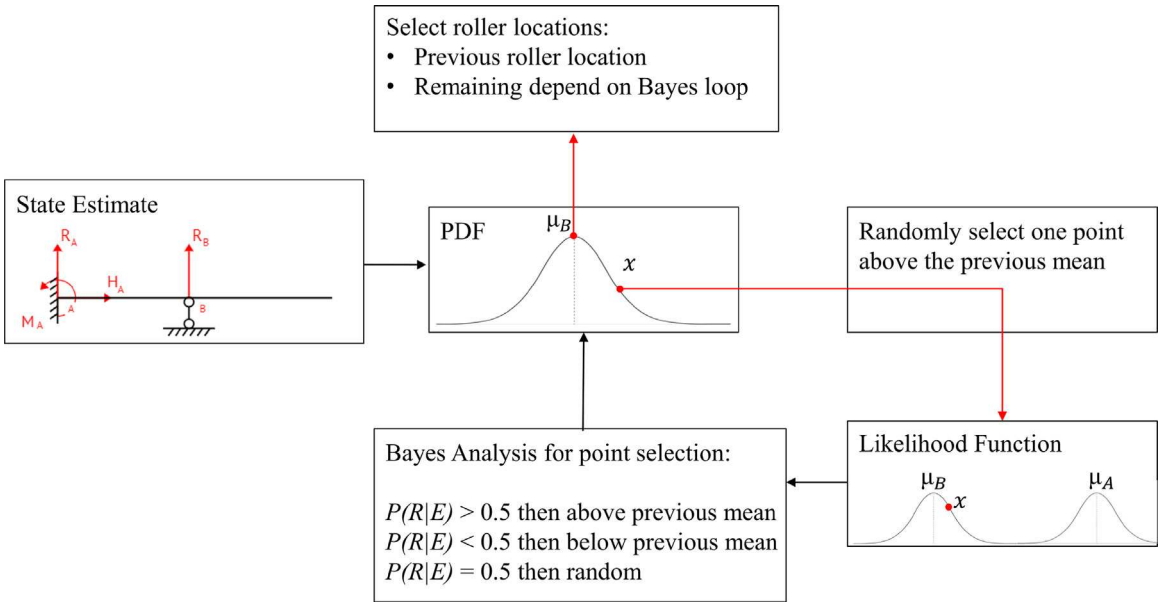

Fig. 13. Analytical application of the likelihood function and Bayes algorithm.

Here, σ is the standard deviation of the position distribution, μ_B is the last estimated roller location, μ_A is the estimated roller location from two iterations ago. If $\mu_B > \mu_A$, the roller was last moving right. If $\mu_A > \mu_B$, then the roller was last moving left. The likelihood function is then used in the Bayes' theorem as follows:

$$P(R \mid E) = \frac{P(R)P(E \mid R)}{P(R)P(E \mid R) + P(L)P(E \mid L)} \tag{41}$$

The output of Eq. (41) is the posterior or updated distribution for the roller location after information regarding the previous location selections and likelihoods are taken into consideration [43]. If $P(R \mid E) > 0.5$, then it is assumed that the roller is currently moving to the right; therefore, the remaining two sample locations are selected from above the previous mean value. If $P(R \mid E) < 0.5$, then it is assumed that the roller is currently moving to the left; therefore, the remaining two sample locations are selected from below the previous mean value. If $P(R \mid E) = 0.5$, then the remaining two sample locations are selected at random.

In summary, the Bayes procedure refines roller positions to select probable locations based on past estimates and uncertainty. The selected points are then used as input for LEMP, which calculates the analytical frequency at each point. The analytical frequencies are then compared to the true experimental frequency to make state estimations, and the analytical loop repeats itself.

3.2. Real-time model updating and model assessment

Real-time model updating can be completed in two steps: (1) calculating the analytical frequency at selected roller positions and (2) choosing the best estimation to represent the current system state using comparison methods. Analytical solutions for system states in this work are calculated using three methods: GE, LEMP, and LEMP with a Bayesian search space. The analytical solutions are used to estimate system states by two methods: error minimization and bounded regression, each using three comparison points. The error minimization method compares the true (measured) frequency with the frequency at the three testing points and selects the location that minimizes absolute error. The bounded regression approach was adopted from Hong et al. [37], where the linear model by least-squares method is given in its general form by Eq. (42) [46].

$$\begin{bmatrix} a \\ b \end{bmatrix} = (\mathrm{X}^{\mathrm{T}}\mathrm{X})^{-1}\mathrm{X}^{\mathrm{T}}\mathrm{Y} \tag{42}$$

When three locations selected for comparison of frequency based on roller location, X and Y are defined as below:

$$\mathrm{X} = \begin{bmatrix} \mathrm{x}_1 & 1 \\ \mathrm{x}_2 & 1 \\ \mathrm{x}_3 & 1 \end{bmatrix} \tag{43}$$

$$\mathrm{Y} = \begin{bmatrix} \omega_1 - \omega_{\mathrm{true}} \\ \omega_2 - \omega_{\mathrm{true}} \\ \omega_3 - \omega_{\mathrm{true}} \end{bmatrix} \tag{44}$$

where a and b are regression parameters such that $\omega - \omega_{\mathrm{true}} = ax + b$. Therefore, $\omega = \omega_{\mathrm{true}}$ when $x = {}^{-b}/_{a}$. However, because errors in the regression model propagate where sample data is limited, the estimated roller location is bound between the minimum and maximum comparison locations as shown:

$$\mathrm{x}_c = \begin{cases} x_{\min} & {}^{-b}/_{a} < x_{\min} \\ x_{\max} & {}^{-b}/_{a} > x_{\max} \\ {}^{-b}/_{a} & \text{elsewhere} \end{cases} \tag{45}$$

The estimated roller displacements are compared to the measured values by mean absolute error (MAE), signal-to-noise ratio (SNR) and Time Response Assurance Criterion (TRAC) to assess the viability of each method. While MAE quantifies the numerical error between the measured and estimated states, the TRAC value quantifies the similarity between time traces [47–49] by comparing the numerical error and time delay of each estimation. The equations for MAE, SNR, and TRAC are shown in Eqs. (46) and (48) respectively.

$$\mathrm{MAE} = \frac{\sum_{i=1}^{z} |x_{\mathrm{true}_i} - x_{\mathrm{est}_i}|}{z} \tag{46}$$

$$\mathrm{SNR}_{\mathrm{dB}} = 10 \log_{10}\left(\frac{P_{\mathrm{signal}}}{P_{\mathrm{noise}}}\right) \tag{47}$$

$$\mathrm{TRAC} = \frac{[\{t_m\}^{\mathrm{T}}\{t_e\}]^2}{[\{t_m\}^{\mathrm{T}}\{t_m\}][\{t_e\}^{\mathrm{T}}\{t_e\}]} \tag{48}$$

where z is the in Eq. (46) is the number of samples used for the state estimation, and t_m and t_e are time traces of the measured and estimated data, respectively. A TRAC value of one indicates perfect time alignment, and a value of zero indicates that the signals have no temporal synchronization (i.e. signals not in phase). Therefore, the ideal model would yield a low MAE value and a TRAC value near one.

In this experimental investigation, the objective is to optimize two parameters; estimation error and iteration time. The number of nodes and the number of FEA models needed to obtain optimum objective parameters can be obtained using the single objective optimization problem formulated as shown in Eq. (49):

$$\begin{aligned} &\underset{\mathbf{P}}{\text{minimize}} \quad \text{fit} = (1-\alpha)\frac{e(\mathbf{P})}{e'} + \alpha\frac{t(\mathbf{P})}{t'} \\ &\text{subject to} \quad \mathbf{P} = [p_{\mathrm{nodes}}, p_{\mathrm{models}}] \in \mathbb{P} \end{aligned} \tag{49}$$

Table 3
Assessment of the error minimization comparison method when solving for 3 FEA models 26 nodes.

Solution type	Mean absolute error (mm)	TRAC	SNR_{dB}
GE	10.280	.959	8.755
LEMP	10.286	.957	8.752
LEMP with Baysian search space	10.320	.959	8.730

Table 4
Assessment of the bounded regression comparison method when solving for 3 FEA models 26 nodes.

Solution type	Mean absolute error (mm)	TRAC)	SNR_{dB}
GE	8.54	.963	9.555
LEMP	11.17	.958	8.392
LEMP with Bayesian search space	10.85	.957	8.518

where $\mathbf{P}$ is the combination of p_{nodes} and p_{models} which are the number of nodes and the number of models used, respectively, and $\mathbb{P}$ is the parameter search space. In this formulation, e is the estimation error, and e' is the maximum desired error, while t and t' are the iteration time and maximum desired time, respectively. α is the scalarization factor and can be selected based on the characteristics of the dynamic environment it is applied to. For a problem with error an minimization focus, α is selected as 0; for an iteration time focus, α would be set to 1. In this manuscript, a value of $\alpha = 0.5$ is selected, along with $e' = 10$ mm and $t' = 1$ ms. An example problem and code are provided in a public repository [50].

4. Results and discussion

This section presents the results and provides a discussion on key considerations.

4.1. Model updating results

Fig. 14 illustrates results for the estimated roller position of the DROPBEAR testbed using the error minimization technique for a 26 node beams with 3 FEA models solved in parallel. Fig. 14(a) presents the estimated roller position using the traditional GE formulation, while Fig. 14(b) shows the results obtained using LEMP. Lastly, Fig. 14(c) reports the estimated roller position obtained using LEMP with Bayesian search space. Initially, it is assumed that the roller is located at the midpoint of the beam and is moving to the right. This assumption accounts for the spike in error at the start of each estimation process. The fluctuation in estimations between Fig. 14(a) and (b) are similar; therefore, it cannot be concluded that LEMP alone provides smooth estimates. However, as seen in Fig. 14(c), implementing a Bayesian search space with LEMP solutions allows for less fluctuation and smoothens the estimates since comparison points are not selected at random but rather by using a probabilistic approach. This is most advantageous when the roller is stationary, as estimates remain constant for the most part.

The mean absolute error between the estimated and true position and the TRAC values obtained using error minimization are shown in Table 3. The GE method has a mean absolute error of 10.280 mm with a TRAC value of 0.9596 compared to LEMP with an error of 10.286 mm with a TRAC value of 0.9577 and LEMP with a Bayesian search space has an error of 10.320 mm, and TRAC value of 0.9592. Fig. 14 shows that the estimated data is improved. However, higher MAE and lower SNR is observed in both LEMP approaches compared to the GE approach because of the overshoot in estimated data when the roller is stationary. Accounting for the overshoot observed in LEMP with Bayesian estimated data will result in a better estimate than GE as the MAE is reduced to 5.65 mm. Therefore, it is concluded that LEMP with Bayesian somewhat improves the estimated value, with the Bayesian approach offering a slightly better estimate.

Fig. 15 illustrates the estimated roller pin location results obtained for the GE, LEMP, and LEMP with a Bayesian search space for a bounded regression approach used as the comparison method. Again, the fluctuation in estimations between Fig. 15(a)–(c) are similar, but there is slightly less fluctuation in the LEMP approach that utilizes a Bayesian search space. The MAE between the estimates using the bounded regression technique and true position, SNR, and the TRAC values for each method are shown in Table 4. The GE method has a mean absolute error of 8.54 mm and TRAC value of 0.9637 compared to LEMP with an error of 11.17 mm and TRAC value of 0.9580 and LEMP with a Bayesian search space with an error of 10.85 mm and TRAC value of 0.9575. As mentioned earlier, the LEMP algorithm will offer better estimation after accounting for the overshoot when the roller is stationary.

Note that the error for LEMP with a Bayesian search space is greater when linear regression is applied than when the error minimization technique is applied. This is due to the conflicting approaches of Bayes and linear regression when the roller is stationary. When minimizing error, the previous location is selected as a roller location and chosen as a state estimation when the roller is stationary. However, for linear regression, the approach creates a line of best fit which might not contain the previous location.

While the error minimization approach yields lower MAE values, there are significant fluctuations in the estimates, which are reduced by applying a Bayesian search space as shown in Fig. 14. The bounded regression method allows estimations of roller

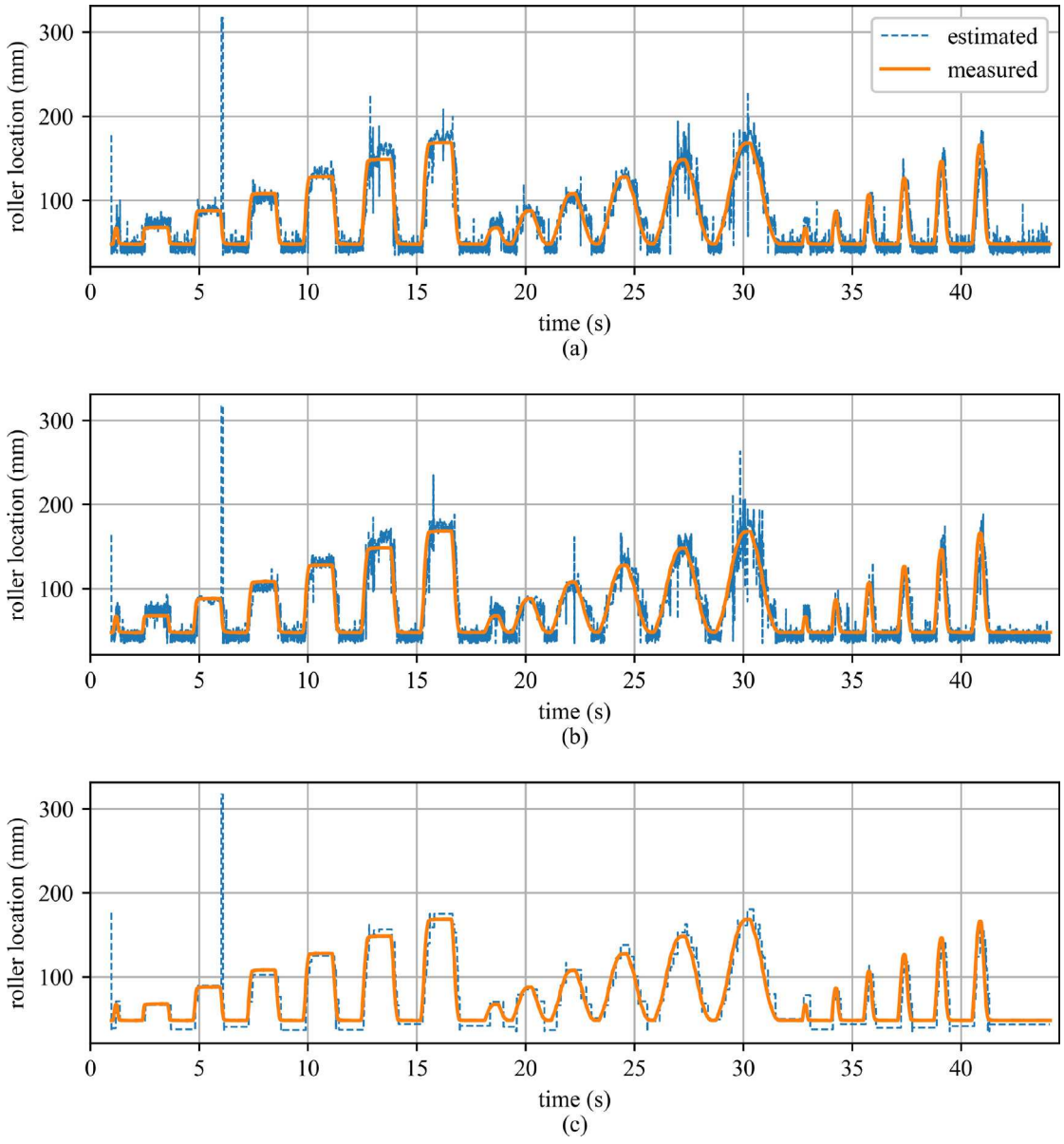

Fig. 14. Roller estimations solved using error minimization by: (a) the traditional GE approach; (b) LEMP estimations, and; (c) LEMP estimations using a Bayesian search space.

locations not located on pre-selected nodes, yielding smoother estimation curves. The one exception is the LEMP estimates using a Bayesian search space for linear regression because of their conflicting nature. In summary, a LEMP approach using a Bayesian search space would perform best using an error minimization technique, while LEMP alone would perform best using a linear regression technique.

4.2. State estimation update time

The LEMP approach offers a lower computational time when compared to solving the GE problem as the structure is simplified through its modal space representation. The state update time for GE, LEMP, and LEMP with the Bayesian search space for several numbers of nodes are investigated in this work; using a computer with a Intel®, Core© i7-10700K processor with a base clock of 3.80 GHz and 64 GB of RAM.

There is a significant difference in timing between the GE solver and the LEMP solver; this is expected as the LEMP algorithm has the new state roots (eigenvalues) bounded to the previous state frequencies, therefore avoiding having to find eigensolutions; which

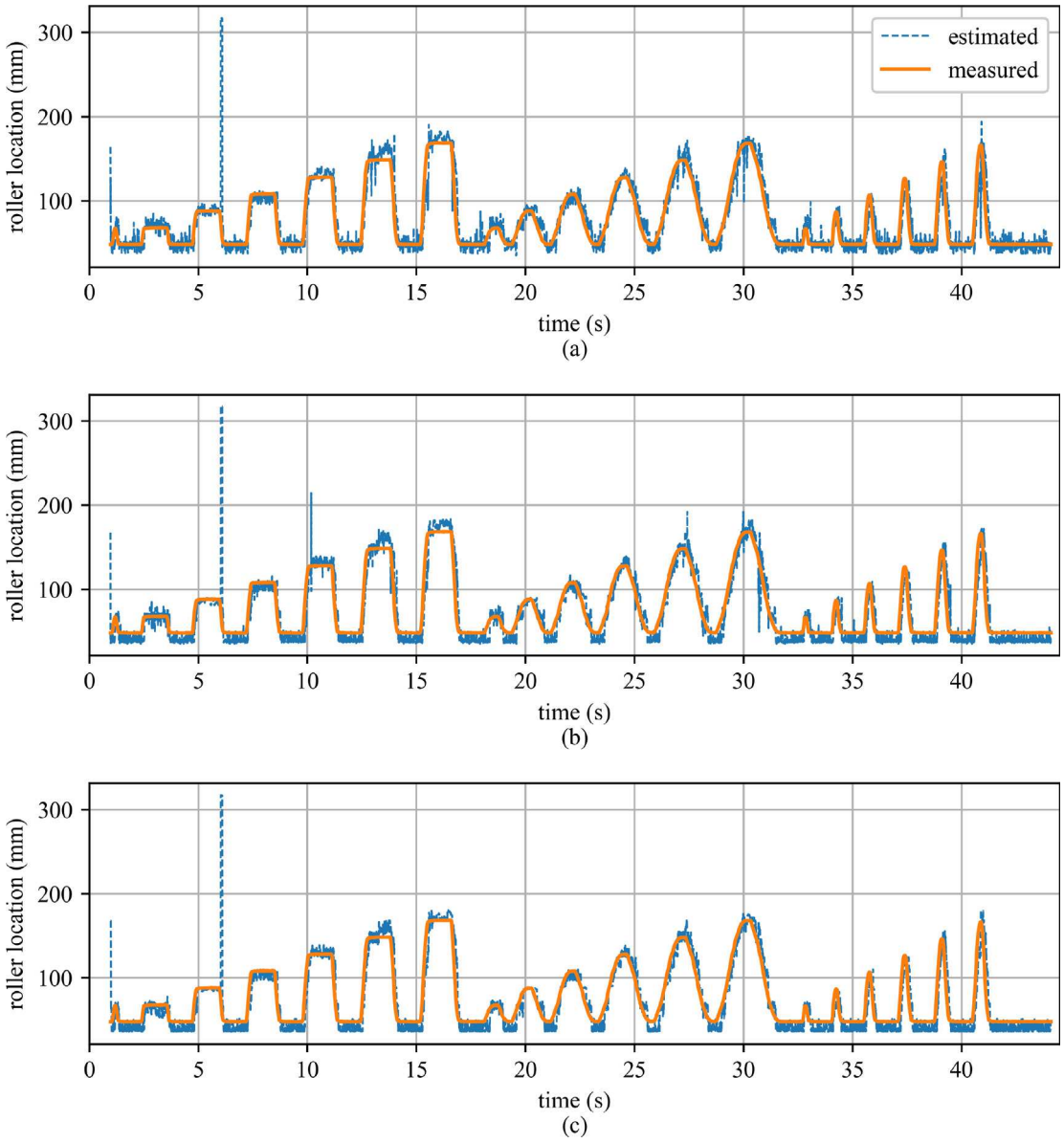

Fig. 15. Roller estimations solved using bounded regression by: (a) the traditional GE approach; (b) LEMP estimations, and; (c) LEMP estimations using a Bayesian search space.

Table 5
Time, MEA, and SNR for LEMP and LEMP with Bayesian using error minimization and bounded regression for three FEA models.

	LEMP								LEMP Bayesian							
	Error minimization				Bounded regression				Error minimization				Bounded regression			
	21	26	51	101	21	26	51	101	21	26	51	101	21	26	51	101
Time	0.251	0.253	0.271	0.306	0.320	0.329	0.342	0.381	0.299	0.305	0.318	0.363	0.370	0.372	0.392	0.444
MEA	12.77	10.28	10.01	9.71	11.72	11.17	10.31	10.20	13.52	10.32	9.97	9.62	12.48	10.85	10.21	9.66
SNR_{dB}	7.811	8.75	9.01	9.52	8.18	8.39	9.23	9.62	7.56	8.73	9.12	9.77	7.90	8.52	9.45	10.12
TRAC	0.954	0.957	0.961	0.972	0.956	0.958	0.960	0.978	0.957	0.959	0.971	0.984	0.956	0.957	0.962	0.971

reduces the computational cost and therefore makes it faster. Fig. 16 presents the solver time details for GE and LEMP up to 250 nodes. Fig. 16(a) shows the time it takes both solvers to solve for a new state frequency for a model with 10 to 250 nodes. The solver here is exclusive to other state update procedures like comparison methods and the addition of Bayesian search space. As presented

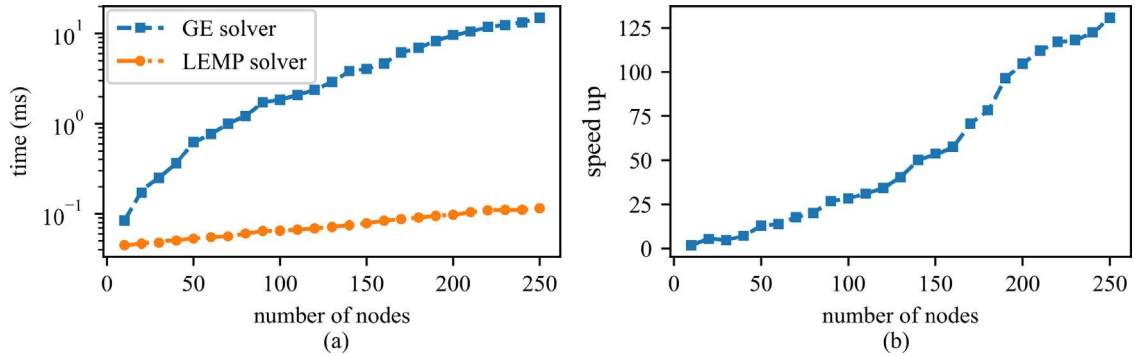

Fig. 16. Solver time for the GE and LEMP showing: (a) the time taken by both solver to solve for new state frequency, and; (b) the ratio between the GE and LEMP solver representing the speed up of the GE.

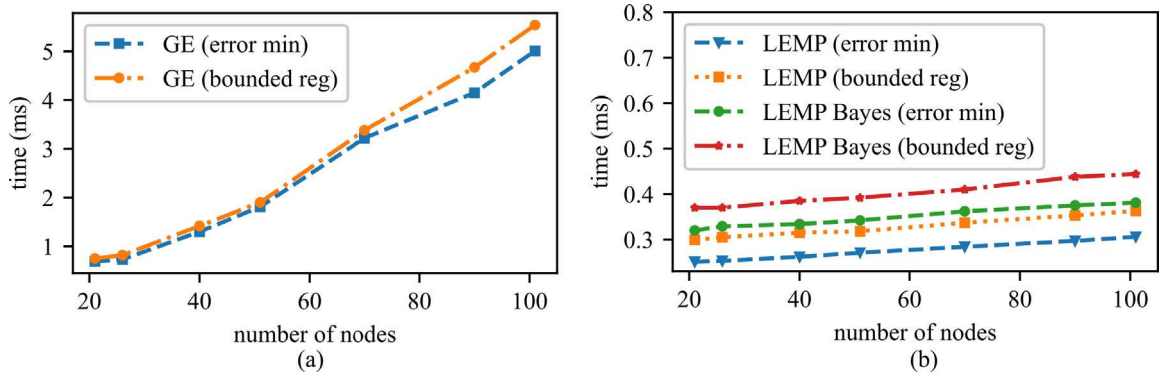

Fig. 17. Iteration(state update) time comparison between the error minimization technique and bounded regression when using: (a) the traditional GE, and; (b) LEMP and LEMP with Bayesian.

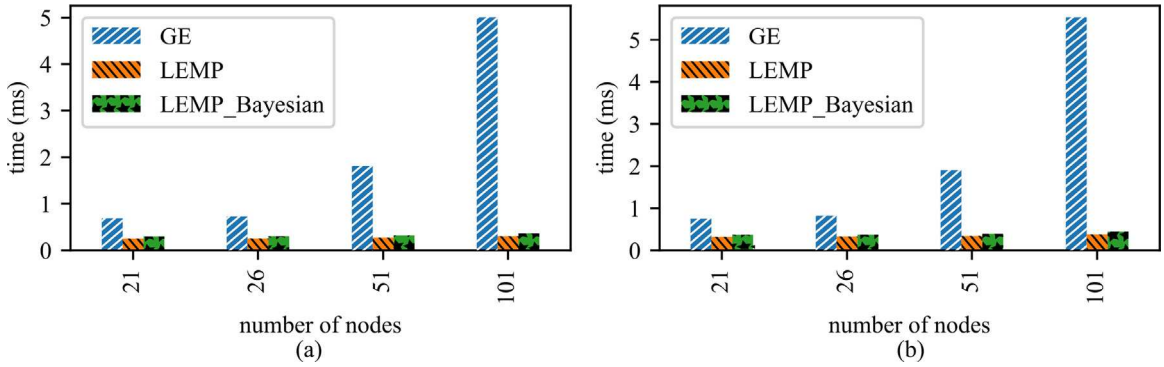

Fig. 18. Iteration (state update) time using different comparison methods showing: (a) error minimization, and; (b) bounded regression.

in Fig. 16(a), the generalized eigenvalue solver takes more time than the LEMP solver. In Fig. 16(b), the data shows the speed up offered by the LEMP solver compared to GE. Between 10 to 250 nodes, the GE solver's time is seen to increase exponentially with a speedup of about 125 times at the 250 node model, which roughly relates to the largest model that can be updated within the 1 ms timing constraint using LEMP. As the number of nodes increases beyond 250, the speedup offered by LEMP will continue to increase.

For the focus nodes of 21, 26, 51, and 101, the GE had a timing of 0.19, 0.24, 0.64, and 1.86 ms, respectively. This result shows that the GE approach would not meet the stringent real-time constraints set by the high-rate dynamic system challenge as the number of nodes increases. On the other hand, the LEMP solver had a timing of 0.045, 0.046, 0.050, and 0.061 ms for 21, 26, 51, and 101 nodes, respectively. This significant time difference is also due to the prioritization of the contributing nodes.

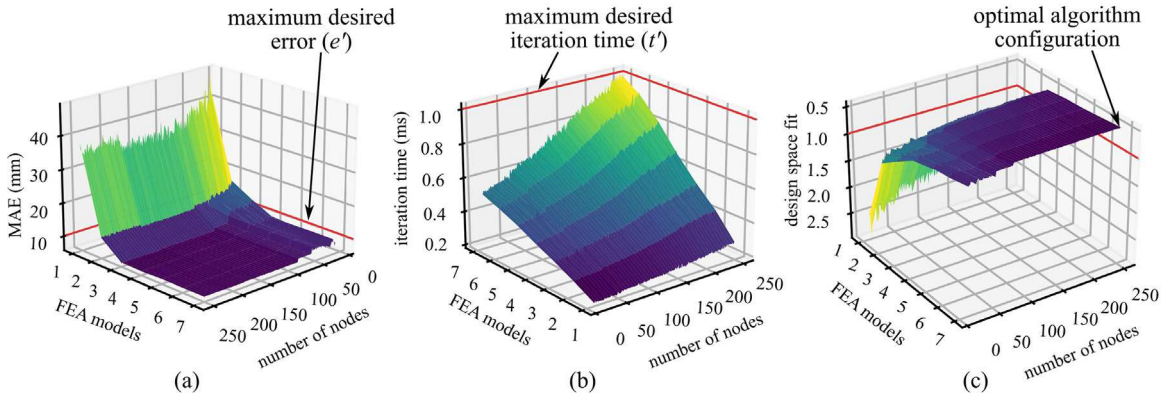

Fig. 19. Figure showing the effect number of nodes and number of sampled roller locations has on (a) the mean absolute error, and; (b) the iteration time using the LEMP algorithm with bounded regression comparison methods.

There was no significant difference in timing between the two comparison methods (error minimization and bounded regression) as shown in Fig. 17(a) and (b). For the GE and LEMP solver, the error minimization technique can perform slightly faster than bounded regression. This is expected as the regression process takes more time than mere error calculations. However, both comparison methods offer advantages when considering the approach to use. Moreover, Fig. 17(b) reports the timing results for LEMP with Bayes estimator. As expected, the addition of the Bayes calculation adds computation cost and, therefore, time to its calculations.

The solver's time alone does not determine how long it will take to update the system's current state. The number of FEA models solved in parallel at each time step, and the comparison method influences the time taken to update the system's state. Fig. 18 shows the time data for three FEA models for both the error minimization technique in Fig. 18(a) and bounded regression in Fig. 18(b). The timing for both approaches is similar; however, the time performance of LEMP against GE is not. The figures show that the time constraint of 1 ms is only met at 21 and 26 nodes when using the GE, whereas, for both LEMP and LEMP with Bayesian, the state update time of 1 ms can be achieved for models with more than 101 nodes.

Fig. 19 reports the performance space for the model updating scheme. Fig. 19(a) shows how the mean absolute error of state estimation is affected by the number of nodes used to build the FEA model of the beam and the number of FEA models solved in parallel. The data shows that the number of FEA models selected will cause the estimation to exceed the allowable error if it is one or two. There is no noticeable reduction in error if the number of FEA models selected is beyond three for nodes between 51 and 101. However, the error when using fewer nodes can be reduced by selecting a higher number of FEA models during the state update process. Fig. 19(b) displays data on how the number of nodes and the number of FEA models solved in parallel affect the iteration time. As the number of nodes increases, the iteration time increases, and the same is seen for the number of FEA models used. Since selecting three FEA models allows the state estimation to stay within the allowable error, it is reasonable to discard the usage of the higher FEA models to reduce computation time. Parameter optimization is carried out as earlier described and shown in Fig. 19(c); an optimal algorithm configuration is seen to be at around 250 nodes with seven FEA models. This optimal algorithm configuration may change on different hardware.

Detailed data on time, mean absolute error, signal-to-noise ratio, and TRAC values on the state estimation results for the LEMP and LEMP with Bayesian with three FEA models solved in parallel for 21, 26, 51, and 101 nodes is presented in Table 5. The data shows that error is decreased as the number of nodes increases, whereas time increases as the number of nodes increases.

5. Summary and conclusion

In this work, a real-time model updating technique that leverages the local eigenvalue modification procedure (LEMP) to reduce the original eigenvalue solution to a set of second-order equations is formulated. Experimental validation was undertaken using data from the DROPBEAR testbed, and the proposed algorithm was implemented offline. For the relatively simplistic structure considered here, modeling errors in the initial formulation of the system were not found to be a challenge.

Roller estimations were calculated by GE solutions, LEMP solutions, and LEMP solutions utilizing a Bayesian search space using both error minimization and linear regression as comparison methods. The error minimization technique generally resulted in sharp transient errors during roller movement and fluctuation when the roller remained stationary. Both of which were improved with the application of a Bayesian search space. Applying the bounded regression technique generally reduced estimation fluctuation during roller movement but not during stationary periods.

The GE and LEMP solutions offered similar accuracy; the LEMP solutions with a Bayesian search space yielded smoother results with less fluctuation during roller movements and stationary periods, which is advantageous when tracking an unchanging system as false reports of damage would be minimal. However, the results also showed that GE would scale poorly with the higher node

when time is a critical factor being considered. Therefore, the LEMP algorithm is used on the DROPBEAR data to update its state under 1 ms for up to 250 nodes.

From this work, it can be inferred that LEMP solutions reduce the number and complexity of calculations required for state estimations. Furthermore, it is shown that LEMP performs best using a linear regression method, while LEMP approaches using a Bayesian search space perform best using an error minimization method. It is concluded from this work that the LEMP approach yields state estimations that are comparable to those found using a GE solution and provide a viable method for updating models in real-time. An example problem and code are provided in a public repository.

Declaration of competing interest

The authors declare that they have no known competing financial interests or personal relationships that could have appeared to influence the work reported in this paper.

Data availability

The data used is shared through a public GitHub repository, as are many of the key components of the code.

Acknowledgments

This material is based upon work supported by the Air Force Office of Scientific Research (AFOSR), United States through award no. FA9550-21-1-0083 and no. FA9550-21-1-0082. This work is also partly supported by the National Science Foundation, United States grant numbers 1850012, 1937535, and 1956071 and by the United States Air Force. This material is partially based upon work supported by the University of South Carolina, United States through grant number 80003212. Any opinions, findings, and conclusions or recommendations expressed in this material are those of the authors and do not necessarily reflect the views of the University of South Carolina, the National Science Foundation, or the United States Air Force (Distribution A. Approved for public release; distribution unlimited (96TW-2021-0061)).

References

[1] J. Hong, S. Laflamme, J. Dodson, B. Joyce, Introduction to state estimation of high-rate system dynamics, Sensors 18 (2) (2018) 217, http://dx.doi.org/10.3390/s18010217.

[2] J. Dodson, A. Downey, S. Laflamme, M.D. Todd, A.G. Moura, Y. Wang, Z. Mao, P. Avitabile, E. Blasch, High-rate structural health monitoring and prognostics: An overview, in: Data Science in Engineering, Volume 9, Springer International Publishing, 2021, pp. 213–217, http://dx.doi.org/10.1007/978-3-030-76004-5_23.

[3] D. Li, Y. Wang, Modal dynamic residual-based model updating through regularized semidefinite programming with facial reduction, Mech. Syst. Signal Process. 143 (2020) 106792, http://dx.doi.org/10.1016/j.ymssp.2020.106792.

[4] G. Comanducci, F. Magalhães, F. Ubertini, Á. Cunha, On vibration-based damage detection by multivariate statistical techniques: Application to a long-span arch bridge, Struct. Health Monit. 15 (5) (2016) 505–524, http://dx.doi.org/10.1177/1475921716650630.

[5] A. Downey, J. Hong, J. Dodson, M. Carroll, J. Scheppegrell, Millisecond model updating for structures experiencing unmodeled high-rate dynamic events, Mech. Syst. Signal Process. 138 (2020) 106551, http://dx.doi.org/10.1016/j.ymssp.2019.106551.

[6] X. Liu, Y. Wang, E.I. Verriest, Simultaneous input-state estimation with direct feedthrough based on a unifying MMSE framework with experimental validation, Mech. Syst. Signal Process. 147 (2021) 107083, http://dx.doi.org/10.1016/j.ymssp.2020.107083.

[7] J. Hong, S. Laflamme, J. Dodson, Study of input space for state estimation of high-rate dynamics, Struct. Control Health Monit. 25 (6) (2018) e2159, http://dx.doi.org/10.1002/stc.2159.

[8] F. Mostert, Challenges in blast protection research, Def. Technol. 14 (5) (2018) 426–432, http://dx.doi.org/10.1016/j.dt.2018.05.007.

[9] J. Richert, D. Coutellier, C. Götz, W. Eberle, Advanced smart airbags: The solution for real-life safety? Int. J. Crashworthiness 12 (2) (2007) 159–171, http://dx.doi.org/10.1080/13588260701433461.

[10] W.-M. Li, J.-Z. Hong, New iterative method for model updating based on model reduction, Mech. Syst. Signal Process. 25 (1) (2011) 180–192, http://dx.doi.org/10.1016/j.ymssp.2010.07.009.

[11] E. Simoen, G.D. Roeck, G. Lombaert, Dealing with uncertainty in model updating for damage assessment: A review, Mech. Syst. Signal Process. 56–57 (2015) 123–149, http://dx.doi.org/10.1016/j.ymssp.2014.11.001.

[12] J. Yan, X. Du, A. Downey, A. Cancelli, S. Laflamme, L. Leifsson, A. Chen, F. Ubertini, Surrogate model for condition assessment of structures using a dense sensor network, in: H. Sohn (Ed.), Sensors and Smart Structures Technologies for Civil, Mechanical, and Aerospace Systems 2018, Vol. 10598, SPIE, 2018, pp. 10598–10599, http://dx.doi.org/10.1117/12.2296711.

[13] C. Rainieri, G. Fabbrocino, E. Cosenza, Near real-time tracking of dynamic properties for standalone structural health monitoring systems, Mech. Syst. Signal Process. 25 (8) (2011) 3010–3026, http://dx.doi.org/10.1016/j.ymssp.2011.04.010.

[14] Z. Yang, L. Wang, Structural damage detection by changes in natural frequencies, J. Intell. Mater. Syst. Struct. 21 (3) (2009) 309–319, http://dx.doi.org/10.1177/1045389x09350332.

[15] R. Astroza, H. Ebrahimian, J.P. Conte, Performance comparison of Kalman-based filters for nonlinear structural finite element model updating, J. Sound Vib. 438 (2019) 520–542, http://dx.doi.org/10.1016/j.jsv.2018.09.023.

[16] Z. Zhang, C. Sun, V. Jahangiri, Structural damage identification of offshore wind turbines: A two-step strategy via FE model updating, Struct. Control Health Monit. 29 (2) (2022) e2872, http://dx.doi.org/10.1002/stc.2872.

[17] J.T. Weissenburger, Effect of local modifications on the vibration characteristics of linear systems, J. Appl. Mech. 35 (2) (1968) 327–332, http://dx.doi.org/10.1115/1.3601199.

[18] Y. Huang, C. Shao, B. Wu, J.L. Beck, H. Li, State-of-the-art review on Bayesian inference in structural system identification and damage assessment, Adv. Struct. Eng. 22 (6) (2018) 1329–1351, http://dx.doi.org/10.1177/1369433218811540.

[19] R. Madarshahian, J.M. Caicedo, Reducing MCMC computational cost with a two layered Bayesian approach, in: Model Validation and Uncertainty Quantification, Volume 3, Springer International Publishing, 2015, pp. 291–297, http://dx.doi.org/10.1007/978-3-319-15224-0_31.

[20] Y. Huang, J.L. Beck, S. Wu, H. Li, Robust Bayesian compressive sensing for signals in structural health monitoring, Comput.-Aided Civ. Infrastruct. Eng. 29 (3) (2014) 160–179, http://dx.doi.org/10.1111/mice.12051.
[21] Y. Zhao, M. Gong, Z. Zuo, Y. Gao, Bayesian estimation approach based on modified SCAM algorithm and its application in structural damage identification, Struct. Control Health Monit. 28 (1) (2021) e2654, http://dx.doi.org/10.1002/stc.2654.
[22] M. Kurata, J.-H. Kim, J.P. Lynch, K.H. Law, L.W. Salvino, A probabilistic model updating algorithm for fatigue damage detection in aluminum hull structures, in: ASME 2010 Conference on Smart Materials, Adaptive Structures and Intelligent Systems, Volume 2, ASMEDC, 2010, http://dx.doi.org/10.1115/smasis2010-3838.
[23] B. Joyce, J. Dodson, S. Laflamme, J. Hong, An experimental test bed for developing high-rate structural health monitoring methods, Shock Vib. 2018 (2018) 1–10, http://dx.doi.org/10.1155/2018/3827463.
[24] A. Downey, J. Hong, J. Dodson, M. Carroll, J. Scheppegrell, Dataset-2-DROPBEAR-acceleration-vs-roller-displacement, 2020, URL https://github.com/High-Rate-SHM-Working-Group/Dataset-2-DROPBEAR-Acceleration-vs-Roller-Displacement.
[25] J. He, Structural modification, Phil. Trans. R. Soc. A 359 (1778) (2001) 187–204, http://dx.doi.org/10.1098/rsta.2000.0720.
[26] A. Sestieri, Structural dynamic modification, Sadhana 25 (3) (2000) 247–259, http://dx.doi.org/10.1007/bf02703543.
[27] E. Lofrano, A. Paolone, G. Ruta, Dynamic damage identification using complex mode shapes, Struct. Control Health Monit. 27 (12) (2020) e2632, http://dx.doi.org/10.1002/stc.2632.
[28] C.-X. Qu, T.-H. Yi, X.-J. Yao, H.-N. Li, Complex frequency identification using real modal shapes for a structure with proportional damping, Comput.-Aided Civ. Infrastruct. Eng. 36 (10) (2021) 1322–1336, http://dx.doi.org/10.1111/mice.12676.
[29] S.D. Bilbao, Numerical Sound Synthesis, first ed., John Wiley & Sons, Ltd, West Sussex, UK, 2009.
[30] S. Bilbao, C. Desvages, M. Ducceschi, B. Hamilton, R. Harrison-Harsley, A. Torin, C. Webb, Physical modeling, algorithms, and sound synthesis: The NESS project, Comput. Music J. 43 (2–3) (2020) 15–30, http://dx.doi.org/10.1162/comj_a_00516.
[31] D. Formenti, M. Richardson, Modal Modeling and Structural Dynamics Modification, Tech. rep., Vibrant Technology, Inc., 2020.
[32] W. Dai, C.P. Yu, J.M. Roesset, Dynamic stiffness matrices for analyses in the frequency domain, Comput.-Aided Civ. Infrastruct. Eng. 22 (4) (2007) 265–281, http://dx.doi.org/10.1111/j.1467-8667.2007.00484.x.
[33] P. Avitabile, Twenty years of structural dynamic modification- A review, Sound Vib. 37 (1) (2003) 14–25.
[34] J. Hallquist, V. Snyder, Synthesis of two discrete vibratory systems using eigenvalue modification, AIAA J. 11 (2) (1973) 247–249, http://dx.doi.org/10.2514/3.6738.
[35] J. Hallquest, Modification and Synthesis of Large Dynamic Structural Systems [Ph. D. Thesis], 1974.
[36] R.J. Allemang, D.L. Brown, Experimental Modal Analysis and Dynamic Component Synthesis, Vol. 1, Flight Dynamics Laboratory, Air Force Wright Aeronautical Laboratories, 1987, URL https://apps.dtic.mil/dtic/tr/fulltext/u2/a195147.pdf.
[37] S.H. Hong, C. Drnek, A. Downey, Y. Wang, J. Dodson, Real-time model updating algorithm for structures experiencing high-rate dynamic events, in: ASME 2020 Conference on Smart Materials, Adaptive Structures and Intelligent Systems, American Society of Mechanical Engineers, 2020, http://dx.doi.org/10.1115/smasis2020-2439.
[38] A. Jesus, P. Brommer, R. Westgate, K. Koo, J. Brownjohn, I. Laory, Modular Bayesian damage detection for complex civil infrastructure, J. Civ. Struct. Health Monit. 9 (2) (2019) 201–215, http://dx.doi.org/10.1007/s13349-018-00321-8.
[39] K.A. Eltouny, X. Liang, Bayesian-optimized unsupervised learning approach for structural damage detection, Comput.-Aided Civ. Infrastruct. Eng. 36 (10) (2021) 1249–1269, http://dx.doi.org/10.1111/mice.12680.
[40] Y. Yuan, F.T. Au, D. Yang, J. Zhang, Active learning structural model updating of a multisensory system based on Kriging method and Bayesian inference, Comput.-Aided Civ. Infrastruct. Eng. (2022) http://dx.doi.org/10.1111/mice.12822.
[41] M. Ebrahimzadeh Hassanabadi, A. Heidarpour, S. Eftekhar Azam, M. Arashpour, A Bayesian smoothing for input-state estimation of structural systems, Comput.-Aided Civ. Infrastruct. Eng. 37 (3) (2022) 317–334, http://dx.doi.org/10.1111/mice.12733.
[42] F.-L. Zhang, C.-W. Kim, Y. Goi, Efficient Bayesian FFT method for damage detection using ambient vibration data with consideration of uncertainty, Struct. Control Health Monit. 28 (2) (2021) e2659, http://dx.doi.org/10.1002/stc.2659.
[43] M. Li, W.Q. Meeker, Application of Bayesian methods in reliability data analyses, J. Qual. Technol. 46 (1) (2014) 1–23, http://dx.doi.org/10.1080/00224065.2014.11917951.
[44] E. Ogunniyi, A.R.J. Downey, J. Bakos, Development of a real-time solver for the local eigenvalue modification procedure, in: D. Zonta, Z. Su, B. Glisic (Eds.), Sensors and Smart Structures Technologies for Civil, Mechanical, and Aerospace Systems 2022, SPIE, 2022, p. 51, http://dx.doi.org/10.1117/12.2613208.
[45] PCB Model 393B04, PCB Piezotronics, 2019.
[46] J. Friedman, T. Hastie, R. Tibshirani, The Elements of Statistical Learning, Vol. 1, Springer series in statistics, New York, 2001.
[47] T. Van Zandt, Development of Efficient Reduced Models for Multi-Body Dynamics Simulations of Helicopter Wing Missile Configurations (Master's thesis), Department of Mechanical Engineering, 2006.
[48] P. Avitabile, P. Pingle, Prediction of full field dynamic strain from limited sets of measured data, Shock Vib. 19 (2012) 765–785, http://dx.doi.org/10.3233/SAV-2012-0686.
[49] T. Van Zandt, N. Wirkkala, P. Avitabile, Development of efficient reduced models for rigid body dynamics simulation for helicopter missile wing combinations, in: Proceedings of the Twenty-Fourth International Modal Analysis Conference, St. Louis, Missouri, 2006, URL http://faculty.uml.edu/pavitabile/downloads/IMAC24_VanZandt_Helicopter_reduced_models_102105.pdf.
[50] E. Ogunniyi, C. Drnek, S.H. Hong, A.R. Downey, Y. Wang, P.A. Jason D. Bakos, J. Dodson, Repository for Real-time Structural Model Updating using Local Eigenvalue Modification Procedure for Application in High-Rate Dynamic Events, GitHub, 2022, URL https://github.com/ARTS-Laboratory/Paper-Real-time-Structural-Model-Updating-using-Local-Eigenvalue-Modification-Procedure.